

The role of processing temperature for achieving superplastic properties in an Al-3Mg-0.2Sc alloy processed by high-pressure torsion

Pedro Henrique R. Pereira ^{a,*}, Piotr Bazarnik ^b, Yi Huang ^{c,d},
Malgorzata Lewandowska ^b, Terence G. Langdon ^c

^aDepartment of Metallurgical and Materials Engineering,
Universidade Federal de Minas Gerais, Belo Horizonte 31270-901, MG, Brazil.

^bFaculty of Materials Science and Engineering, Warsaw University of Technology,
Woloska 141, 02-507 Warsaw, Poland.

^cMaterials Research Group, Department of Mechanical Engineering,
University of Southampton, Southampton SO17 1BJ, U.K.

^dDepartment of Design and Engineering, Faculty of Science and Technology,
Bournemouth University, Poole, Dorset BH12 5BB, U.K.

Abstract

Experiments were conducted to systematically assess the superplastic properties and the microstructural changes of an Al-3Mg-0.2Sc alloy processed by 10 HPT revolutions at room temperature (RT \approx 300 K) or at 450 K after subsequent tensile testing at temperatures from 473 to 723 K over a wide range of strain rates. The HPT processing at RT led to the development of elongated grains with an average size of \sim 140 nm whereas the grain structures were equiaxed and slightly larger (\sim 150 nm) after HPT at 450 K. After HPT processing at RT, the Al-Mg-Sc alloy exhibited true superplastic flow at low homologous temperatures and attained a maximum elongation of \sim 850 % at 523 K. Nevertheless, the elongations decreased at temperatures $T \geq 623$ K and an elongation higher than 400 % was only achieved at 673 K for a strain rate of $\dot{\epsilon} = 4.5 \times 10^{-3} \text{ s}^{-1}$. The material processed by HPT at 450 K displayed superior microstructural stability and substantially higher superplastic ductilities. Elongations of > 1100 % were attained at 673 K for strain rates from 3.3×10^{-4} to $1.0 \times 10^{-1} \text{ s}^{-1}$ and a record elongation of \sim 1880 % for an HPT-processed metal was achieved at $1.5 \times 10^{-2} \text{ s}^{-1}$ at 673 K. High strain rate superplasticity was also reached for an extended range of temperatures and strain rates. Analysis of the data confirms a stress exponent of \sim 2 which is consistent with superplastic flow by grain boundary sliding accommodated by dislocation glide and climb.

Keywords: Aluminium alloys; Grain boundary sliding; High-pressure torsion; Superplasticity; Ultrafine grains.

*Corresponding author: Pedro Henrique R. Pereira (ppereira@demet.ufmg.br)

1. Introduction

The processing of alloys through severe plastic deformation (SPD) procedures has been extensively evaluated over the last three decades in order to fabricate metals with ultrafine grain sizes [1–4]. These materials usually exhibit improved mechanical strength and superplastic properties by comparison with their counterparts prepared using conventional metal-working procedures where this is due to the exceptional levels of grain refinement introduced during SPD processing [3]. Although various SPD processes are now available, major focus has been devoted to the procedures of equal-channel angular pressing (ECAP) [5] and high-pressure torsion (HPT) [6,7] using anvils having quasi-constrained configurations [8,9]. Both techniques require relatively simple apparatus and they permit the processing of difficult-to-work materials by controlling the imposed pressure and the temperature in the work-pieces [10–12]. In practice, HPT processing is more effective than ECAP because it leads to both smaller grain sizes [13,14] and larger fractions of grain boundaries having high angles of misorientation [15].

As the strain rate in superplasticity is inversely proportional to the square of the grain size [16], SPD processing produces nanostructured metals that may be used for superplastic forming at faster production rates [17–20]. In this context, the Al-Mg-Sc alloys have attracted significant attention due to their enhanced microstructural stability [21–25] which is promoted by the precipitation of nanosized Al₃Sc particles [26–29]. This could potentially permit the application of this alloy as aircraft components exposed to temperatures up to ~573 K for short periods to replace traditional Al-Li alloys or heavier materials such as titanium alloys [27]. It has been recently demonstrated that Al-Mg-Sc alloys reach yield stresses >600 MPa after HPT [25,30]. It was also revealed that even after exposure to temperatures up to 623 K for 1 h the yield strength remains higher than 300 MPa [25]. Accordingly, the Al-Mg-Sc alloys consistently achieve high strength at low temperatures [25,30] and excellent superplastic ductilities after SPD [31].

Although numerous studies have highlighted the excellent mechanical properties of Al-Mg-Sc alloys, their widespread commercial use remains limited due to the relatively high cost of scandium (Sc) additions. For this reason, these Sc-containing aluminium alloys are predominantly utilized in specialized applications where performance outweighs material cost considerations, such as in aerospace components and in the automotive industry [27,32].

The superplastic properties of Al-Mg-Sc alloys have been extensively examined after ECAP [21,33–37]. For example, an Al-3Mg-0.2Sc alloy processed by 8 ECAP passes at room temperature (RT) attained an elongation of ~2580 % after tensile testing at $3.3 \times 10^{-3} \text{ s}^{-1}$ at 723 K [33]. Similarly, an Al-Mg-Sc-Zr alloy displayed an even higher ductility after processing by ECAP at the high temperature of ~600 K with a maximum elongation of ~4100 % in tensile deformation at 723 K [36]. Although these results demonstrate that the processing of Al-Mg-Sc alloys through ECAP at high temperatures permits the achievement of superior superplastic ductilities, the reasons for this behaviour are not fully understood.

It has been shown that finer grain structures are produced in Al-Mg-Sc alloys by HPT processing than by ECAP [38–40] but, nevertheless, this is not supported by higher elongations in tensile testing at high temperatures [38,41]. The lower tensile elongations recorded in samples processed by HPT are generally attributed to the utilisation of miniature specimens or at least to specimens cut from discs having relatively small thicknesses [38,40,42,43]. Furthermore, the microstructures developed during HPT at RT are less thermally stable than after ECAP [21,25,44], and grain coarsening can potentially reduce the superplastic properties at high temperatures and low strain rates.

These observations motivated the current research to provide a more comprehensive understanding of the superplastic behaviour of Al-Mg-Sc alloys after processing by HPT. It is important to note that higher superplastic elongations were

reported for the Mg–9Al [45] and AZ61 [46] alloys after processing by HPT at elevated temperatures and recent investigations revealed a remarkable enhancement in the thermal stability of the Al-3Mg-0.2Sc alloy after undertaking the HPT processing at ~450 K [24,25,47]. Thus, it appears that this strategy has the potential of enhancing the superplastic properties of Al-Mg-Sc alloys after HPT processing.

Accordingly, the present research was conducted to evaluate the flow properties and microstructural changes of an Al-3Mg-0.2Sc alloy after processing through 10 turns of HPT at 300 or 450 K and subsequently testing in tension at temperatures from 473 to 723 K. The overall objective was to determine the range of strain rates and temperatures in which this alloy exhibits true superplastic flow and to identify the optimum deformation conditions for attaining tensile elongations that are adequate for achieving reasonably rapid superplastic forming.

2. Experimental material and procedures

An Al-3% Mg-0.2% Sc (in wt. %) alloy was used in this research. This material was supplied by China Rare Metal Material Corporation (Jiangxi Province, China) as forged billets with diameters of ~10 mm. The billets were solution treated at 880 ± 2 K for 1 h and then quenched in water to maximise the Sc content in solid solution and thereby produce a uniform array of grains with an average size of ~300 μm . Thereafter, the bars were cut in the form of discs and then ground to thicknesses of ~0.8 mm.

These Al-3Mg-0.2Sc discs were processed by HPT either at RT \approx 300 K (HPT-RT) or at 450 ± 5 K (HPT-HT) where this corresponds to homologous temperatures (T_H) of ~0.3 and ~0.5, respectively. As documented in earlier studies [25,45,47,48], a processing temperature of ~450 K was attained by using a heating element encircling the massive anvils. The temperature was controlled by inserting a thermocouple within a specially designed hole in the upper anvil such that the tip of the temperature sensor was positioned at a distance of ~10 mm from the upper surface of the HPT disc. The HPT

samples were initially compressed within the depression of the quasi-constrained anvils [49–51] until a nominal pressure of 6 GPa was achieved. They were then subjected to torsional straining up to 10 HPT turns using a rotation rate of ~1 rpm.

The HPT-processed discs were ground to the mid-thickness positions and finally they were polished using 0.06 μm silica colloidal. Vickers hardness measurements were recorded along the entire surfaces of the polished samples using an FM300 microhardness tester under a load of ~200 gf and a dwell time of 15 s. As in an earlier study [52], the measurements followed a rectilinear grid with indentations separated by 0.3 mm and the individual hardness values were then used to construct colour-coded contour maps.

As reported earlier [25,48,53–55], two off-centre miniature tensile specimens, having widths and gauge lengths of ~1.0 and 1.1 mm, respectively, were machined from each HPT-processed disc using electrical discharge wire cutting. After processing, the surfaces of the discs became curved due to the elastic distortion of the anvils [56]. Therefore, in order to remove any irregularities, the surfaces of the HPT-processed samples were ground and polished to a thickness of ~0.6 mm. Tensile tests were conducted using a Zwick Z030 testing machine over wide ranges of strain rates ($\dot{\epsilon}$) and temperatures (T) varying from 3.3×10^{-4} to 1.0 s^{-1} and 473 to 723 K, respectively. The procedure involved clamping the miniature specimens within specially designed grips and then assembling the grips and specimen in the testing machine equipped with a tubular furnace. The miniature specimens were held in a hot chamber for ~10 min to permit temperature stabilisation and thereafter pulled to failure at a constant rate of cross-head displacement with the temperature held constant to within ± 2 K during testing. The tensile tests were conducted at least in duplicate for each individual temperature and strain rate condition to ensure the reproducibility of the results. A M420 stereoscope was used to obtain images of the fractured specimens and to measure the final lengths in the gauge sections of the samples.

Following tensile testing, observations of the surfaces of the fractured specimens were undertaken using a JSM6500F thermal field emission scanning electron microscope (SEM) operating at 15 kV. The secondary electron (SE) images were used to measure the average grain boundary spacing (\bar{L}) in the gauge sections of the tested specimens using the linear intercept method. The microstructures of the Al-3Mg-0.2Sc alloy tensile tested at selected strain rates at 673 K were also examined using transmission electron microscopy (TEM) with a JEOL 1200EX microscope operating at 200 kV and through orientation imaging microscopy using electron backscattered diffraction (EBSD). The EBSD scans were conducted at the grip and within the gauge areas of the fractured specimens with a minimum step size of 0.09 μm whereas the TEM examinations were performed on lamellas extracted by focused ion beam along the gauge sections. The EBSD mappings were conducted at an operating voltage of 15 kV using tilt angles and working distances of 60° and ~15 mm, respectively. Orientation maps were generated from each EBSD scan, and these results were used to analyse the distributions of the correlated misorientation angles and the grain diameters measured using the equivalent circle method.

The microstructures of the HPT-processed discs were investigated through scanning transmission electron microscopy (STEM) using a Hitachi 5500 microscope operating at 30 kV. Discs of ~3 mm diameter were punched at distances of ~3.5 mm from the centres of the HPT discs and then twin-jet electropolished with 70% CH₃OH and 30% HNO₃ at ~250 K using a Struers Tenupol-5 system.

3. Experimental Results

3.1 Vickers microhardness and microstructure after HPT

Fig. 1 shows colour-coded contour maps for the distributions of the Vickers hardness over the surfaces of Al-Mg-Sc discs processed by 10 HPT turns at RT and 450 K. As noted earlier [47,57], the unprocessed Al-3Mg-0.2Sc alloy displayed a fairly

uniform hardness distribution with an average value of ~ 60 Hv. After 10 HPT revolutions at RT the microhardness distribution in Fig. 1 is a doughnut-like pattern containing an outer ring of higher hardness values in the range of ~190-210 Hv whereas the central area shows lower hardness values within the interval of ~110-150 Hv.

It is readily apparent from Fig. 1 that the microhardness distribution is more homogenous after processing at 450 K although the hardness values are lower and mostly lie within the range of ~170-190 Hv. These results are consistent with recent results demonstrating that the same Al-Mg-Sc alloy exhibits yield strengths of ~600 and 550 MPa after HPT at 300 and 450 K, respectively [25]. Thus, the local mechanical strength after HPT at different temperatures, as represented by the Vickers hardness values, shows similar percentage differences compared with the yield strengths measured after tensile testing using miniature specimens.

The dislocation and grain structures of representative Al-Mg-Sc microstructures obtained after processing through 10 HPT revolutions are depicted in the STEM images presented in Fig. 2. Average grain sizes of ~140 and ~150 nm were calculated for the Al-3Mg-0.2Sc alloy after HPT at RT and 450 K, respectively, although the grain structures appeared more elongated after processing at RT. A more thorough examination of Fig. 2 reveals the presence of sparse dislocations within some of the grains which are mostly isolated as shown in detail in Figs 2 (b) and (d).

These findings are consistent with both the TEM and the EBSD results documented in a recent report [25]. For example, it was demonstrated that there is no precipitation of nano-sized Al₃Sc particles in the solution-treated Al-3Mg-0.2Sc alloy when HPT processing up to 10 turns. Furthermore, the dislocation density estimated through Rietveld refinement of X-Ray diffraction profiles of the alloy processed by up to 10 HPT revolutions at 300 K was ~5× higher than after processing at 450 K.

3.2 Tensile properties at high temperatures

Fig. 3 shows representative plots of true stress vs true strain for the Al-3Mg-0.2Sc alloy processed through 10 HPT turns at either 300 or 450 K and subsequently tested in tension at 523 or 673 K using strain rates from 3.3×10^{-4} to 1.4 s^{-1} . As in recent studies [48,58], the plots were obtained by converting the load and displacement data into true stress and true strain by considering uniform deformation along the gauge sections of the miniature specimens. Accordingly, although the values of true stress at strains beyond the maximum load do not reflect the precise flow behaviour, the maximum true stress obtained in each test probably provides a better estimate of the load bearing capacity of the microstructures developed at the later stages of testing as further documented in the discussion section.

The results in Fig. 3 demonstrate that the HPT-HT material consistently exhibits lower flow stresses and higher elongations than the same alloy processed by HPT at RT for tensile tests carried out at comparable temperatures and strain rates. For both processing temperatures, it is also emphasized that the flow behaviour of the HPT-processed alloy at high temperatures strongly depends upon the strain rates. For tests conducted at 523 K, it is apparent that the material processed at 450 K reaches lower flow stresses and higher maximum strains than the HPT-RT metal for $\dot{\epsilon} \geq 10^{-2} \text{ s}^{-1}$. Nonetheless, specimens tested at 523 K using lower strain rates display very similar ductilities although the latter require higher yield stresses.

Inspection of Fig. 3 reveals that increasing the testing temperature from 523 to 673 K promotes a marked decrease in the flow stresses regardless of the HPT temperature. There is a significant increase in the ductility for the alloy processed at 450 K as follows from the attainment of $\epsilon > 2.5$ for strain rates from 3.3×10^{-4} to 10^{-1} s^{-1} . Conversely, it is shown that the specimens of the HPT-RT material fail at similar or even lower strains at 673 K compared with the testing temperature of 523 K. It is important to emphasize that the alloy processed by HPT at 450 K reaches a maximum strain of ~ 2.4 when tested at

673 K with a strain rate of $3.3 \times 10^{-1} \text{ s}^{-1}$ and this was not achieved for the HPT-RT specimens under any testing condition in Figs 3 (a) and (b). Furthermore, the HPT-HT material exhibits a more significant work hardening during testing at 673 K than the alloy processed by HPT at 300 K.

Fig. 4 displays the appearance of the deformed specimens of the Al-3Mg-0.2Sc alloy after tensile testing and pulling to failure for the same conditions presented in Fig. 3. The values of the elongations to failure ($\Delta l/l_0$) are shown on the right-hand side of the fractured samples where Δl and l_0 are the change in length and the initial gauge length, respectively. Examination of Fig. 4 demonstrates that the HPT-RT samples tested in tension at 523 K achieved elongations $> 400 \%$ for $\dot{\epsilon} \leq 1.4 \times 10^{-2} \text{ s}^{-1}$ revealing the occurrence of both superplastic flow which requires an elongation of at least 400 % [59] and the advent of high strain rate superplasticity which occurs at strain rates at and above 10^{-2} s^{-1} [60]. Furthermore, the general lack of any visible incipient necking within the gauge lengths of the specimens processed by HPT at 450 K confirms the occurrence of quasi-stable plastic flow and true superplasticity [61].

Nevertheless, it is noted that an increase in the testing temperature to 673 K consistently leads to a reduction in the tensile ductility such that for the material processed by HPT at RT there is an elongation of $\Delta l/l_0 > 400 \%$ only at $\dot{\epsilon} \approx 4.5 \times 10^{-4} \text{ s}^{-1}$. A more detailed inspection of the fractured specimens in Fig. 4 (a) shows that the HPT-RT specimens develop very diffuse necking during testing at 673 K for $\dot{\epsilon} \leq 4.5 \times 10^{-3} \text{ s}^{-1}$ as the widths of the samples are reasonable constant along the entire gauge lengths. By contrast, there is a sharper width gradient for the HPT-RT samples tested at 523 K even though the material then reaches higher elongations.

The results in Fig. 4 (b) demonstrate reliably that the Al-Mg-Sc alloy processed by HPT at 450 K exhibits greater ductility than after processing by HPT at 300 K. High strain rate superplasticity is achieved during testing at 523 K for strain rates as high as

$1.0 \times 10^{-1} \text{ s}^{-1}$. Additionally, the HPT-HT alloy achieves extraordinarily high elongations for all testing strain rates at 673 K with a maximum elongation of 1880 % when testing with a strain rate of $1.5 \times 10^{-2} \text{ s}^{-1}$. This represents the highest elongation achieved to date in conventional Al alloys subjected to HPT processing [31,62,63] and it exceeds the earlier record-breaking elongation of 1600% reported for the same alloy processed by HPT for 2 revolutions at RT when samples of ~1 mm in thickness were subjected to tensile testing at 573 K using a strain rate of $3.3 \times 10^{-3} \text{ s}^{-1}$ [40]. It should be noted also that elongations $\geq 980 \%$ were recorded for the HPT-HT specimens when testing at 673 K at all strain rates over the range from 3.3×10^{-4} to $3.3 \times 10^{-1} \text{ s}^{-1}$.

To better visualize the variation of the tensile elongations with the strain rate and temperature, Fig. 5 shows plots of the $\Delta l/l_0$ values vs strain rate for the Al-3Mg-0.2Sc alloy processed by 10 HPT turns at (a) RT and (b) 450 K for tensile tests conducted at temperatures from 473 to 723 K. Fig. 5 (a) shows that the HPT-RT material achieves an elongation of ~560 % when pulled to failure at 473 K for $\dot{\epsilon} = 1.4 \times 10^{-3} \text{ s}^{-1}$ but increasing the temperature to 573 K leads to a general enhancement of ductility. Nevertheless, the tensile elongations decrease significantly when increasing the temperature to 673 K.

The plots in Fig. 5 (b) demonstrate that the alloy processed by HPT at 450 K exhibits superior superplastic properties such that elongations $>400 \%$ were achieved for tests performed at 473 K with $\dot{\epsilon} \leq 3.3 \times 10^{-2} \text{ s}^{-1}$. The elongations tend to increase with increasing temperatures with maximum values at 673 K and slightly lower elongations at 723 K. It is important to note that elongations higher than 600 % were consistently obtained for all tests conducted at strain rates ranging from 3.3×10^{-4} to 10^{-2} s^{-1} .

Fig. 6 shows plots of the variation of the flow stress at $\epsilon = 0.3$ with the strain rate for the alloy processed by 10 HPT turns at two different temperatures and tested in tension using various strain rates at temperatures from 473 to 723 K. The experimental data were

plotted using logarithmic scales for both the stress and the strain rate so that the local slopes of these curves represent the apparent strain rate sensitivity, m .

It is apparent from Fig. 6 (a) that the plots of the HPT-RT alloy indicate two separate slopes depending on the strain rate and temperature. For tests at 473 K there is a value of $m \approx 0.5$ for $\dot{\epsilon} < 10^{-2} \text{ s}^{-1}$ and a slope of ~ 0.22 at faster strain rates. Furthermore, the range of strain rates with $m \approx 0.5$ expands towards faster strain rates ($\sim 4.5 \times 10^{-2} \text{ s}^{-1}$) with increasing temperatures up to $T \approx 623 \text{ K}$.

A comparison of Figs 6 (a) and (b) shows that the alloy processed at 473 K displays markedly lower flow stresses at $\epsilon = 0.3$ than after HPT at RT. The curves of the HPT-HT metal at 473 and 523 K exhibit a sigmoidal profile with a slope of ~ 0.5 at intermediate strain rates. The curves in Fig. 6 (b) show $m \geq 0.5$ for $T \geq 573 \text{ K}$ considering $\dot{\epsilon} \geq 10^{-2} \text{ s}^{-1}$. However, these slopes decrease at lower strain rates and the HPT-HT alloy exhibits m values of $\sim 0.2-0.3$ at temperatures from 573 to 673 K and $\dot{\epsilon} < 10^{-2} \text{ s}^{-1}$. It should be noted that the HPT-HT alloy achieves higher flow stresses during deformation at 723 K than at 673 K for $\dot{\epsilon} \geq 10^{-2} \text{ s}^{-1}$.

3.3 Microstructures after deformation at high temperatures

Fig. 7 shows typical orientation maps and the corresponding $\{111\}$ pole figures taken along (a) the undeformed area and (b) the gauge section of the specimens processed by HPT at RT and tested in tension at 673 K with a strain rate of $4.5 \times 10^{-2} \text{ s}^{-1}$. Examination of Fig. 7 (a) reveals the onset of abnormal coarsening at the grip area of the miniature specimen during heating at 673 K for the period of $\sim 660 \text{ s}$ when considering the total time the sample was held within the tensile testing apparatus. This is consistent with a recent study where the same alloy underwent secondary recrystallisation and extensive grain growth after heating at either 623 or 673 K for 1 h [25]. This microstructure displays fine grains together with a population of grains having sizes of tens of micrometres with the $\{100\}$ planes nearly parallel to the thickness direction.

By contrast, the grains in the gauge section are predominantly oriented with the $\{110\}$ planes parallel to the thickness direction. It should be noted that these grains are elongated towards the tensile axis and contain a substantial fraction of low-angle grain boundaries (LAGBs) with misorientation angles ranging from 2-15° and which are often organised in the form of subgrains. The grain structures in the gauge area of the specimen are slightly finer than in the undeformed section and measurements for each orientation map gave values of the average grain size, \bar{L} , of ~2.2 and ~2.5 μm in the undeformed and gauge section, respectively.

Histograms detailing the distributions of grain diameters and the fraction of correlated boundaries as a function of the misorientation angles are presented in Fig. 1A of the Supplementary Material. They reveal that the gauge section of the specimen has a narrower distribution of grain diameters although there is evidence of bimodal distributions of grain diameters for both areas. The histograms of the misorientation angles for the HPT-RT alloy are noticeably different from the Mackenzie distribution shown by the solid line in Fig. 1A (b) [64] and this may be attributed to the development of a preferential texture and substructures. The deformed and the undeformed areas of the samples have fractions of LAGBs of ~26 and 22 %, respectively, and these values are higher than the fraction measured after HPT at RT [25].

Fig. 8 shows orientation maps and the corresponding $\{111\}$ pole figures taken at the undeformed areas and the gauge sections of the fractured specimens of the alloy originally processed by HPT at 450 K and then tested in tension at 673 K using various strain rates. The lines coloured in white denote $\Sigma 3$ 60° $\langle 111 \rangle$ twin boundaries. Inspection shows that abnormal coarsening gradually evolves in the undeformed areas of the HPT-HT alloy as specimens are tested at slower strain rates and the consequent exposure to the testing temperature for longer periods of time leads to larger grain sizes. In contrast with the HPT-RT material, the deformed areas of the fractured specimens have grains with

larger sizes than their undeformed counterparts and the microstructures display very few LAGBs.

The gauge section of the material tested at 1.0 s^{-1} in Fig. 8 (b) shows a weaker texture than the undeformed area but there is an increase in the fraction of grains with a texture component around $\{110\}$. There is also evidence for the development of an essentially random texture during testing at $3.3 \times 10^{-2} \text{ s}^{-1}$ for the alloy in Fig. 8 (d) processed by HPT at 450 K. Furthermore, after tensile testing at $3.3 \times 10^{-4} \text{ s}^{-1}$ in Fig. 8 (f) the grains in the HPT-HT sample exhibit higher aspect ratios than after deformation at faster strain rates and there is some evidence for twinning activity and the onset of abnormal grain growth. Similar histograms were constructed for the HPT-RT metal tested at 673 K and they are presented in Fig. 2A of the Supplementary Material corresponding to the orientation maps shown in Fig. 8.

It is well established that, due to the occurrence of grain boundary sliding, the grains become elevated above the surfaces of specimens during straining under superplastic conditions [48,65,66]. For this reason, a thorough examination of the surface topography of the fractured samples permits measurement of the grain sizes in the HPT-processed alloy after tensile testing. Several SE images were taken along the deformed areas of the fractured specimens and examples are shown in Fig. 3A of the Supplementary Material for the samples tested at 673 K after processing at (a) 300 and (b) 450 K. These images were used to estimate the grain sizes after tensile testing and to thereby analyse the grain growth kinetics under dynamic conditions. The results are presented in Fig. 9 as plots of grain size vs time at testing temperature for the Al-3Mg-0.2Sc alloy processed by HPT at RT or 450 K and tested in tension at temperatures from 473 to 723 K.

It is readily apparent from Fig. 9 that the material processed by HPT at RT displays faster kinetics of grain coarsening than the material processed by HPT at 450 K under comparable conditions of tensile testing. After straining at 473 K, all specimens continue

to exhibit ultrafine-grained (UFG) structures even after prolonged exposure times of ~4 h. There is a substantial increase in grain size after raising the temperature from 473 to 523 K although the grain sizes in the HPT-HT alloy are smaller. Further increases in temperature produce minor coarsening for the material processed by HPT at 450 K but the grain sizes increase markedly for the HPT-RT material deformed at $T \geq 573$ K.

To investigate whether high temperature straining leads to the development of second phases in the HPT-processed alloy, TEM observations were undertaken along the gauge sections of the miniature specimens of the Al-3Mg-0.2Sc alloy originally subjected to 10 HPT revolutions at either 300 or 450 K and then tested at 673 K using similar strain rates. Typical results are shown in Fig 10 in which the TEM images on the left were obtained using transfer electron (TE) contrast but the micrographs on the right were from atomic number (Z) contrast.

For both processing temperatures, it is readily apparent that there is a profuse distribution of second phase particles in the vicinity of the grain boundaries of the HPT-processed alloy. These second phases were identified as Al₃Sc precipitates using electron dispersive spectroscopy and the electron diffraction patterns (see Figs 4A and 5A in the Supplementary Material). These phases appear to display smaller sizes and cover large amounts of the grain boundaries in the HPT-HT material compared with the alloy processed by HPT at 300 K. Furthermore, the Al₃Sc particles appear to be in a later stage of coalescence in the latter material and they form relatively thick films along the grain boundaries of the grains having sizes of ~1-2 μm .

4. Discussion

4.1 Superplastic characteristics after HPT

Fig. 11 shows colour-coded maps that were constructed using the data from Fig. 5 to plot the variations in elongation with temperature and strain rate where the broken lines added to these plots delineate the contours where there is an elongation of at least

400 %. Following the earlier definition of superplastic flow [59], these broken lines therefore represent the onset of true superplasticity at the slower strain rates. The maps of temperature vs strain rate in Fig. 11 provide a new procedure for depicting the superplastic data and careful analysis shows the trends are generally consistent with the reported results for many other superplastic ultrafine-grained materials [67]. It follows from Fig. 11 that the alloy processed through 10 HPT revolutions at 473 K displays remarkable ductility compared with the samples processed by HPT at RT. The HPT-HT material reached high elongations for all testing conditions examined in this research and exhibited true superplastic ductilities over an extended range of temperatures and strain rates. In general, the elongation values for the HPT-HT alloy increase with increasing temperature up to $T \approx 673$ K where elongations higher than 1000 % were achieved for tests conducted at $\sim 3.3 \times 10^{-4} \leq \dot{\epsilon} \leq 3.3 \times 10^{-1} \text{ s}^{-1}$. There is also consistent evidence that the superplastic properties of the alloy processed by HPT at RT deteriorate at $T \geq 623$ K.

In superplastic materials the variation of elongation with strain rate shows a peak at intermediate strain rates [68–70]. The true stress vs true strain curves at superplastic conditions often show a sigmoidal shape which allows the classification of three distinct deformation regimes. At extremely high strain rates (region III), the contribution of grain boundary sliding (GBS) to the total straining decreases and intragranular dislocation processes are more prominent. This leads to a reduction in the strain rate sensitivity and thus the achievement of lower elongations at faster strain rates. By contrast, the decrease in strain rate occurs concurrently with more intense grain coarsening at very low strain rates (region I). The increase in grain size and the formation of subgrain structures are detrimental for GBS and favours the onset of internal cavities at the grain boundaries which ultimately leads to premature failure during tensile testing.

At an intermediate range of strain rates (region II), there is an optimum condition in which the material achieves enhanced superplastic properties. Within this deformation

regime, the material is capable of retaining ultrafine-grained structures and the recovery kinetics are sufficiently fast to efficiently accommodate GBS by dislocation climb into the opposite grain boundaries. As a consequence, it exhibits higher m values and thus superior ductility. Also, the strain rate sensitivity tends to increase with temperature concurrently with the recovery kinetics and the superplastic ductility. Nonetheless, this effect is counteracted by grain coarsening and the formation of subgrains which adversely affect the action of GBS and may lead to premature failure. Accordingly, in the current study the optimum condition for superplasticity was achieved for the Al-Mg-Sc alloy processed by HPT at 450 K for tests carried out at 673 K and at $1.5 \times 10^{-2} \text{ s}^{-1}$.

The superplastic behaviour observed in this alloy processed by HPT at 450 K is intrinsically associated with its improved thermal stability compared with the HPT-RT material. It is demonstrated in Fig. 9 that the HPT-HT material is capable of retaining fine grain structures for prolonged times during tensile testing at high temperatures. This is consistent with the coarsening kinetics during static annealing as reported in earlier studies [25,47,57]. Also, the presence of precipitates influences superplastic behaviour, as the Zener pinning effect more effectively hinders grain boundary migration when the particles are smaller and more uniformly distributed [71,72].

The results in Fig. 10 reveal that the Al_3Sc particles are substantially smaller and more dispersed in the Al-Mg-Sc alloy processed by HPT at 450 K even though the total time at the testing temperature was ~ 1430 s, whereas the Al alloy processed by HPT at RT was exposed to the testing temperature of 673 K for only ~ 540 s. Accordingly, superplastic flow will occur at faster rates in the material processed by HPT at 450 K as it preserves the smaller grains and thereby exhibits a higher density of HAGBs which are then available to undergo GBS during deformation at high temperatures [16,62,67].

It is worth noting that the material processed by HPT at RT was reported to have a large fraction of grains with $\bar{L} > 10 \text{ }\mu\text{m}$ after heating at 623 and 673 K [25]. These

structures have a large fraction of LAGBs as shown in Fig. 7. In addition, even though the HPT-RT specimens continue exhibiting fine grain structures capable of deforming by GBS, this mechanism may not be operative in the abnormally coarse grains which will probably deform by dislocation glide and climb in the tensile tests performed at faster strain rates. For this reason, the decrease in the elongations in the HPT-RT material tested at $\dot{\epsilon} \geq 4.5 \times 10^{-2} \text{ s}^{-1}$ and at $T \geq 623 \text{ K}$ is attributed directly to the reduced contributions from GBS in the overall straining.

This conclusion is supported by the orientation maps corresponding to the gauge section of the HPT-RT alloy deformed at 673 K as it shows many grains having the {110} planes parallel to the thickness direction which is a common feature for FCC metals strained under non-superplastic conditions [73]. Furthermore, these grains are elongated along the tensile direction and this is not consistent with the occurrence of straining by Rachinger GBS [74,75] which is the fundamental mechanism of superplastic flow [16]. Finally, the plots in Fig. 6 (a) demonstrate that the range of strain rates with $m \approx 0.22$ increases for $T \geq 623 \text{ K}$ and this suggests that dislocation climb becomes predominant at these testing conditions in accordance with the results presented in an earlier study for a coarse-grained Al-Mg-Sc alloy tested over many orders of magnitude of strain rate [44].

It follows from Fig. 6 that the HPT-HT alloy exhibits lower flow stresses than the HPT-RT alloy. However, it is noted that the apparent strain rate sensitivity tends to be < 0.5 in these samples for tests conducted at $\dot{\epsilon} \leq 10^{-2} \text{ s}^{-1}$ although the specimens consistently attained superplastic elongations. It should be noted, however, that these values need to be evaluated with caution as for each corresponding testing temperature grain coarsening tends to be more prominent at slower deformation rates and thus prolonged testing times [76,77]. For this reason, the grain sizes of the Al-Mg-Sc alloy at the same testing temperature are essentially different for the datum points recorded at the equivalent strain of 0.3 for each individual strain rate. Accordingly, the following section

proposes a more adequate model to describe the superplastic flow in the HPT- processed Al alloy.

4.2 The mechanism of flow under superplastic conditions

The strain rate under steady-state conditions during superplastic flow at high temperatures is given by the following expression [16]:

$$\dot{\varepsilon} = \frac{AD_{gb}G\mathbf{b}}{kT} \left(\frac{\mathbf{b}}{d}\right)^2 \left(\frac{\sigma}{G}\right)^2 \quad (1)$$

where A is a dimensionless constant having a value of ~ 10 for conventional metals, D_{gb} is the grain boundary diffusion coefficient, G is the shear modulus, \mathbf{b} is the Burgers vector, k is Boltzmann's constant, d is the spatial grain size given by $d = 1.74 \bar{L}$ [78] and

$$D_{gb} = D_{o,gb} e^{\left(-\frac{Q_{gb}}{kT}\right)} \quad (2)$$

where $D_{o,gb}$ is a frequency factor and Q_{gb} , is the activation energy for grain boundary diffusion.

To identify whether the rate-controlling flow process in all HPT samples displaying elongations of $\Delta l/l_0 \geq 400$ % is GBS, the temperature and grain size compensated strain rate $(\dot{\varepsilon}kT/D_{gb}G\mathbf{b})(d/\mathbf{b})^2$ was plotted against the normalized stress (σ/G) in Fig. 12. These plots were constructed considering σ as the maximum flow stress and d as the spatial grain size in the fractured metal. As in earlier studies [48,62,67,79,80], the calculations used values of $D_{o,gb} = 1.86 \times 10^{-4} \text{ m}^2 \text{ s}^{-1}$, $Q_{gb} = 86 \text{ kJ mol}^{-1}$, $G \text{ (MPa)} = (3.022 \times 10^4) - 16T$ [81] and $\mathbf{b} = 2.86 \times 10^{-10} \text{ m}$ [81]. The solid line labelled $\dot{\varepsilon}_{sp}$ shows the theoretical prediction for superplasticity controlled by grain boundary sliding accommodated by dislocation glide within the grains and subsequent climb into the opposite grain boundaries [16]. Also, additional data were included in Fig. 12 for various superplastic Al-Mg-Sc alloy processed by HPT [38,41,42].

It is readily apparent from Fig. 12 that the experimental values from both the current research and the earlier studies [38,41,42] are consistent with the predictions from

the theoretical model for GBS in superplasticity although many of these values tend to lie slightly above $\dot{\epsilon}_{sp}$. Nevertheless, as indicated in Fig. 12 and from results plotted in a recent review for this Al-Mg-Sc alloy [31], experimental datum points for the alloy processed by ECAP and HPT at RT generally lie below $\dot{\epsilon}_{sp}$. This is a direct consequence of the thermally unstable Al-Mg-Sc microstructures developed after processing at RT since the grain sizes were taken from measurements performed immediately after the SPD processing.

It is important to note that the results obtained after conventional metal-working processes are generally more consistent with the theoretical predictions because these materials display less pronounced grain coarsening during superplastic straining. In the present research, the calculations considered the maximum flow stress and the spatial grain size along the gauge area of the fractured specimens. This means that, although grain growth occurred concurrently with pronounced work hardening during the tensile testing, the present procedure gave a more accurate assessment of the rate-controlling mechanism during superplasticity.

4.3 The influence of subgrain formation on the accommodation process during GBS

There are increases in the fractions of LAGBs organised as subgrains in the HPT-RT metal during deformation at 673 K. Accordingly, in addition to the effect of grain coarsening, there are slower accommodation rates during GBS due to a hindrance in dislocation glide by the subgrain boundaries [82] and this may also contribute to the reduction in ductility observed in the HPT-RT alloy at $T \geq 623$ K. To analyse if there is any correlation between the presence of subgrains and the elongations achieved in this study, Fig. 13 shows the variation of the values of \bar{L} with the normalized stress, σ/G , for the alloy tested in tension after processing by HPT for 10 turns at (a) 300 and (b) 450 K, respectively, where the solid line represents the prediction for the equilibrium subgrain size, λ , in Al-Mg alloys estimated as $\lambda = 20 \mathbf{b} (\sigma/G)^{-1}$ [44,83,84].

Examination of Fig. 13 shows that, as anticipated based on the theoretical analysis [16], for all samples giving superplastic elongations there is a value of $\bar{L} < \lambda$. This is consistent with the orientation maps in Fig. 8 as subgrains are nearly absent in the HPT-HT alloy after testing at 673 K for $\dot{\epsilon} \leq 3.3 \times 10^{-2} \text{ s}^{-1}$. Thus, GBS is easily accommodated by dislocation glide under these conditions and this permits the achievement of extensive superplastic ductilities. By contrast, $\bar{L} > \lambda$ for the HPT-RT alloy tested in tension at 673 K for $\dot{\epsilon} > 4.5 \times 10^{-4} \text{ s}^{-1}$, as confirmed in Fig. 7 (b) for $\dot{\epsilon} = 4.5 \times 10^{-2} \text{ s}^{-1}$, and accordingly the accommodating intragranular slip occurs at slower rates and this ultimately promotes premature failure during tensile testing due to the occurrence of internal cavitation [82]. This failure mode is more likely to occur during deformation at slower strain rates which is consistent with the nearly uniform widths of the fractured specimens deformed at 673 K for $\dot{\epsilon} \leq 4.5 \times 10^{-3} \text{ s}^{-1}$ as shown in Fig. 4 (a).

It also follows from Figs 11 and 13 that elongations $> 400\%$ were not always achieved in the HPT-processed alloy at testing conditions where $\bar{L} < \lambda$ and this is because GBS is thermally-activated so that the sliding rates of adjacent HAGBs increase with increasing temperatures. Although the lack of subgrains facilitates the advent of accommodation during superplasticity, GBS requires exceptionally small grain sizes to operate during deformation at fast strain rates and low temperature [85,86]. In addition, the existence of second phase particles along the grain boundaries makes sliding more difficult and these particles appear to have larger sizes for the HPT-RT alloy deformed at 673 K as shown in Fig. 10.

4.4 An examination of the total elongations achieved in tensile testing

It is important to emphasize that the Al-3Mg-0.2Sc alloy used in this research achieved exceptionally high elongations for an HPT-processed material during deformation at 673 K with an elongation of $\sim 1880\%$ at this temperature for a strain rate of $\dot{\epsilon} = 1.5 \times 10^{-2} \text{ s}^{-1}$ as shown in Fig. 4 (b). This is the highest elongation reported for any

material after conventional HPT processing when tensile tests were conducted using miniature samples cut from the discs with initial thicknesses of ~0.6 mm. Nevertheless, in comparing the tensile elongations achieved using different processing techniques, it is important to note that earlier experiments showed conclusively that the measured elongations in tensile testing were dependent upon the initial overall dimensions of the specimens. Specifically, it was established that higher elongations may be achieved by using specimens having reduced gauge lengths and larger thicknesses [87,88].

In order to demonstrate and understand the reasons underlying the relatively lower ductilities encountered in Al-Mg-Sc alloys after HPT when compared with processing by ECAP, miniature tensile specimens having the same dimensions utilised in the current research were subjected to tensile testing at 523 K and at a strain rate of $\sim 10^{-3} \text{ s}^{-1}$ [24,31]. The results consistently revealed that the elongations attained after HPT at 450 K were $\sim 2\times$ higher than after ECAP. It has been shown that the Al alloy processed by HPT at 450 K exhibits smaller grain sizes and lower hardness after tensile testing than the ECAP-processed alloy. This confirms that HPT processing at 450 K permits the achievement of superior superplasticity at this temperature range due to its enhanced stability.

Also, this set of experiments with miniature tensile specimens was carried out over a wider range of temperatures and strain rates [44]. Although superplastic elongations of $\sim 1880 \%$ were achieved using conventional tensile specimens for the same alloy after ECAP at RT followed by tensile testing at 673 K and at $3.3 \times 10^{-2} \text{ s}^{-1}$ [33], the maximum elongation reached in a miniature specimen under comparable processing and testing conditions was $\sim 980 \%$. Conversely, an elongation to failure of $\sim 1780 \%$ was achieved in the current study for a miniature specimen of the Al-3Mg-0.2c alloy after HPT at 450 K and subsequent tensile testing at 673 K and at $3.3 \times 10^{-2} \text{ s}^{-1}$. This confirms the intrinsic influence of sample size on the elongations achieved under superplastic conditions. It should be further noted that the comparably lower flow stress values at 673 K are

consistent with the enhanced ductility encountered after HPT at 450 K compared with after HPT at RT or even ECAP at RT.

Earlier experiments on an $\text{Al}_9(\text{CoCrFeMnNi})_{91}$ high-entropy alloy processed by HPT showed that it was possible to achieve an elongation of 2000% at 1073 K using a strain rate of $5 \times 10^{-2} \text{ s}^{-1}$ [89] but the specimen thickness was 0.7 mm which is larger than in the present investigation. There are also reports of high elongations of 2580% in an Al-3Mg-0.2Sc alloy [33] and 4100% in an Al-5Mg-0.2Sc alloy [36] but these samples were processed by ECAP where the tensile samples have thicknesses of 2 mm or larger. Finally, it is noted that an elongation to failure of 2320% was reported at a temperature of 298 K for a Bi-43Sn alloy [90] where the sample was processed using the new procedure of tube high-pressure shearing (t-HPS) [91] and the experiments were undertaken using tensile specimens having thicknesses of ~2 mm [92]. Based on this analysis, it is apparent that the maximum elongation of 1880% achieved in the present study is exceptionally large when considering the very thin gauge thickness of ~0.6 mm which severely limits the number of grains available in the specimen cross-section.

4.5 The role of processing temperature on the microstructural evolution during HPT

The Al-3Mg-0.2Sc alloy processed by HPT at RT exhibits slightly elongated grain structures with an average size of ~140 nm. It also displays a dislocation density of $\sim 3.6 \times 10^{13} \text{ m}^{-2}$ as reported in a recent study [25]. These microstructural features are consistent with earlier experiments performed using Al-Mg-Sc alloys processed by SPD at low homologous temperatures [38,42,93,94]. At this range of temperature and strain rate, the restoration mechanism during severe plastic deformation is mechanically-driven which gives rise to grains having higher aspect ratios [95–97].

After HPT at ~450 K, the same Al alloy displays a homogenous array of equiaxed grains with a mean size of ~150 nm, but a considerably lower dislocation density of $\sim 0.7 \times 10^{13} \text{ m}^{-2}$ [25]. It is thus apparent that the restoration mechanism which permits the

achievement of a steady state grain size in the Al-3Mg-0.2Sc alloy during HPT processing at ~450 K is prominently assisted by dynamic recovery. This is consistent with its relative low density of dislocations and the nearly equiaxed grain structures, as obtained in a recent study performed with an Al-Mg-Sc-Zr alloy processed by HPT at 473 K [30].

It should be noted also that the material processed by 10 HPT turns at RT exhibits a broader distribution of grain sizes and sharper gradients in the distributions of extrinsic dislocations throughout the Al microstructure. As demonstrated in detail in an earlier investigation [25], these microstructural features provide conditions for grain boundary migration at faster rates in the material processed by HPT at RT which also shows a more intense susceptibility for abnormal grain coarsening.

The excellent superplastic behaviour achieved in the current investigation is attributed to the enhanced microstructural stability which was promoted by undertaking the HPT processing at 473 K [25]. Thus, this permitted the preservation of an extremely small grain size in the Al-Mg-Sc microstructure and these grains co-existed with a larger proportion of HAGBs and more dispersed Al₃Sc precipitates compared with the material processed by HPT at RT.

5. Summary and conclusions

1- An Al-3Mg-0.2Sc alloy was processed through 10 turns of HPT at RT \approx 300 K and at 450 K to produce a homogeneous array of grains with average sizes of ~140 and 150 nm, respectively. The HPT-processed material was then subjected to tensile testing over a wide range of strain rates and temperatures.

2- Superplastic elongations > 400 % were achieved in the alloy processed by HPT at 300 K during deformation at temperatures up to 573 K and a maximum elongation of ~850 % was achieved at 523 K with a strain rate of $\dot{\epsilon} = 4.5 \times 10^{-3} \text{ s}^{-1}$. Nevertheless, the tensile elongations decreased for tests conducted at $T \geq 623 \text{ K}$ due to extensive grain coarsening.

3- The alloy processed by HPT at 450 K showed enhanced low temperature superplasticity with elongations $> 900\%$ for tests conducted at 573 K for $3.3 \times 10^{-3} \leq \dot{\epsilon} \leq 1.0 \times 10^{-1} \text{ s}^{-1}$. High strain rate superplasticity was attained over an extended range of strain rates. These results are due to the exceptionally small grain sizes and the low fractions of LAGBs in the alloy during deformation at low temperatures.

4- The material processed by HPT at 473 K exhibited optimum superplastic ductilities at 673 K and a record elongation of $\sim 1880\%$ was achieved at this temperature at $\dot{\epsilon} = 1.5 \times 10^{-2} \text{ s}^{-1}$ for an Al-based alloy processed by HPT. Superplastic elongations $\geq 980\%$ were attained at 673 K for $\dot{\epsilon} \leq 3.3 \times 10^{-1} \text{ s}^{-1}$. This enhanced superplasticity originated from a combination of the high diffusion rates at 673 K and the retention of microstructures with very fine grains having larger proportions of HAGBs.

5- Analysis of the data confirms a stress exponent of ~ 2 for the HPT-processed material during superplastic flow demonstrating that flow occurs by GBS accommodated by dislocation glide and climb. The high elongations occur when the grain size remains smaller than the equilibrium subgrain size. The absence of subgrains under these conditions was confirmed by orientation maps and this facilitates accommodation by intragranular slip during GBS.

Data availability

The raw/processed data required to reproduce these findings can be shared upon request.

Acknowledgements

This research was supported by FAPEMIG under Grant APQ-01342–21 (PHRP), the European Research Council under ERC Grant Agreement No. 267464-SPDMETALS (TGL and YH) and CNPq under Grant No. 443736/2018–9 (PHRP).

References

- [1] R.Z. Valiev, R.K. Islamgaliev, I.V. Alexandrov, Bulk nanostructured materials from severe plastic deformation, *Prog Mater Sci* 45 (2000) 103–189. [https://doi.org/10.1016/S0079-6425\(99\)00007-9](https://doi.org/10.1016/S0079-6425(99)00007-9).
- [2] T.G. Langdon, Twenty-five years of ultrafine-grained materials: Achieving exceptional properties through grain refinement, *Acta Mater* 61 (2013) 7035–7059. <https://doi.org/10.1016/j.actamat.2013.08.018>.
- [3] K. Edalati, A. Bachmaier, V.A. Beloshenko, Y. Beygelzimer, V.D. Blank, W.J. Botta, K. Bryła, J. Čížek, S. Divinski, N.A. Enikeev, Y. Estrin, G. Faraji, R.B. Figueiredo, M. Fuji, T. Furuta, T. Grosdidier, J. Gubicza, A. Hohenwarter, Z. Horita, J. Huot, Y. Ikoma, M. Janeček, M. Kawasaki, P. Král, S. Kuramoto, T.G. Langdon, D.R. Leiva, V.I. Levitas, A. Mazilkin, M. Mito, H. Miyamoto, T. Nishizaki, R. Pippan, V. V. Popov, E.N. Popova, G. Purcek, O. Renk, Á. Révész, X. Sauvage, V. Sklenicka, W. Skrotzki, B.B. Straumal, S. Suwas, L.S. Toth, N. Tsuji, R.Z. Valiev, G. Wilde, M.J. Zehetbauer, X. Zhu, Nanomaterials by severe plastic deformation: review of historical developments and recent advances, *Mater Res Lett* 10 (2022) 163–256. <https://doi.org/10.1080/21663831.2022.2029779>.
- [4] R.Z. Valiev, I. V. Alexandrov, M. Kawasaki, T.G. Langdon, *Ultrafine-Grained Materials*, TMS/Springer Nature, Cham, Switzerland, 2024. <https://doi.org/10.1007/978-3-031-31729-3>.
- [5] R.Z. Valiev, T.G. Langdon, Principles of equal-channel angular pressing as a processing tool for grain refinement, *Prog Mater Sci* 51 (2006) 881–981. <https://doi.org/10.1016/J.PMATSCI.2006.02.003>.
- [6] A.P. Zhilyaev, T.G. Langdon, Using high-pressure torsion for metal processing: Fundamentals and applications, *Prog Mater Sci* 53 (2008) 893–979. <https://doi.org/10.1016/j.pmatsci.2008.03.002>.
- [7] K. Edalati, Z. Horita, A review on high-pressure torsion (HPT) from 1935 to 1988, *Materials Science and Engineering A* 652 (2016) 325–352. <https://doi.org/10.1016/j.msea.2015.11.074>.
- [8] A. Hohenwarter, A. Bachmaier, B. Gludovatz, S. Scheriau, R. Pippan, Technical parameters affecting grain refinement by high pressure torsion, *International Journal of Materials Research* 100 (2009) 1653–1661. <https://doi.org/10.3139/146.110224>.
- [9] P.H.R. Pereira, R.B. Figueiredo, Finite element modelling of high-pressure torsion: An overview, *Mater Trans* 60 (2019) 1139–1150. <https://doi.org/10.2320/matertrans.MF201906>.
- [10] R.B. Figueiredo, P.R. Cetlin, T.G. Langdon, The processing of difficult-to-work alloys by ECAP with an emphasis on magnesium alloys, *Acta Mater* 55 (2007) 4769–4779. <https://doi.org/10.1016/j.actamat.2007.04.043>.
- [11] P.H.R. Pereira, R.B. Figueiredo, Y. Huang, P.R. Cetlin, T.G. Langdon, Modeling the temperature rise in high-pressure torsion, *Materials Science and Engineering A* 593 (2014) 185–188. <https://doi.org/10.1016/j.msea.2013.11.015>.

- [12] K. Edalati, Y. Hashiguchi, P.H.R. Pereira, Z. Horita, T.G. Langdon, Effect of temperature rise on microstructural evolution during high-pressure torsion, *Materials Science and Engineering A* 714 (2018) 167–171. <https://doi.org/10.1016/j.msea.2017.12.095>.
- [13] A.P. Zhilyaev, B.K. Kim, G. V. Nurislamova, M.D. Baró, J.A. Szpunar, T.G. Langdon, Orientation imaging microscopy of ultrafine-grained nickel, *Scr Mater* 46 (2002) 575–580. [https://doi.org/10.1016/S1359-6462\(02\)00018-0](https://doi.org/10.1016/S1359-6462(02)00018-0).
- [14] A.P. Zhilyaev, G. V. Nurislamova, B.K. Kim, M.D. Baró, J.A. Szpunar, T.G. Langdon, Experimental parameters influencing grain refinement and microstructural evolution during high-pressure torsion, *Acta Mater* 51 (2003) 753–765. [https://doi.org/10.1016/S1359-6454\(02\)00466-4](https://doi.org/10.1016/S1359-6454(02)00466-4).
- [15] J. Wongsangam, M. Kawasaki, T.G. Langdon, A comparison of microstructures and mechanical properties in a Cu–Zr alloy processed using different SPD techniques, *J Mater Sci* 48 (2013) 4653–4660. <https://doi.org/10.1007/s10853-012-7072-0>.
- [16] T.G. Langdon, A unified approach to grain boundary sliding in creep and superplasticity, *Acta Metallurgica et Materialia* 42 (1994) 2437–2443. [https://doi.org/10.1016/0956-7151\(94\)90322-0](https://doi.org/10.1016/0956-7151(94)90322-0).
- [17] R.Z. Valiev, D.A. Salimonenko, N.K. Tsenev, P.B. Berbon, T.G. Langdon, Observations of high strain rate superplasticity in commercial aluminum alloys with ultrafine grain sizes, *Scr Mater* 37 (1997) 1945–1950. [https://doi.org/10.1016/S1359-6462\(97\)00387-4](https://doi.org/10.1016/S1359-6462(97)00387-4).
- [18] Z. Horita, M. Furukawa, M. Nemoto, A.J. Barnes, T.G. Langdon, Superplastic forming at high strain rates after severe plastic deformation, *Acta Mater* 48 (2000) 3633–3640. [https://doi.org/10.1016/S1359-6454\(00\)00182-8](https://doi.org/10.1016/S1359-6454(00)00182-8).
- [19] A.J. Barnes, Superplastic Forming 40 Years and Still Growing, *J Mater Eng Perform* 16 (2007) 440–454. <https://doi.org/10.1007/s11665-007-9076-5>.
- [20] J. Wongsangam, T.G. Langdon, Advances in superplasticity from a laboratory curiosity to the development of a superplastic forming industry, *Metals (Basel)* 12 (2022) 1921. <https://doi.org/10.3390/MET12111921>.
- [21] S. Lee, A. Utsunomiya, H. Akamatsu, K. Neishi, M. Furukawa, Z. Horita, T.G. Langdon, Influence of scandium and zirconium on grain stability and superplastic ductilities in ultrafine-grained Al–Mg alloys, *Acta Mater* 50 (2002) 553–564. [https://doi.org/10.1016/S1359-6454\(01\)00368-8](https://doi.org/10.1016/S1359-6454(01)00368-8).
- [22] D.G. Morris, M.A. Muñoz-Morris, Microstructure of severely deformed Al–3Mg and its evolution during annealing, *Acta Mater* 50 (2002) 4047–4060. [https://doi.org/10.1016/S1359-6454\(02\)00203-3](https://doi.org/10.1016/S1359-6454(02)00203-3).
- [23] Y.L. Duan, G.F. Xu, X.Y. Peng, Y. Deng, Z. Li, Z.M. Yin, Effect of Sc and Zr additions on grain stability and superplasticity of the simple thermal–mechanical processed Al–Zn–Mg alloy sheet, *Materials Science and Engineering: A* 648 (2015) 80–91. <https://doi.org/10.1016/j.msea.2015.09.049>.
- [24] P.H.R. Pereira, Y. Huang, T.G. Langdon, Thermal stability and superplastic behaviour of an Al–Mg–Sc alloy processed by ECAP and HPT at different

- temperatures, *IOP Conf Ser Mater Sci Eng* 194 (2017) 012013. <https://doi.org/10.1088/1757-899X/194/1/012013>.
- [25] P.H.R. Pereira, P. Bazarnik, Y. Huang, M. Lewandowska, T.G. Langdon, Flow behaviour and microstructural stability in an Al-3Mg-0.2Sc alloy processed by high-pressure torsion at different temperatures, *Materials Science and Engineering: A* 887 (2023) 145766. <https://doi.org/10.1016/j.msea.2023.145766>.
- [26] E.A. Marquis, D.N. Seidman, Nanoscale structural evolution of Al₃Sc precipitates in Al(Sc) alloys, *Acta Mater* 49 (2001) 1909–1919. [https://doi.org/10.1016/S1359-6454\(01\)00116-1](https://doi.org/10.1016/S1359-6454(01)00116-1).
- [27] J. Røyset, N. Ryum, Scandium in aluminium alloys, *International Materials Reviews* 50 (2005) 19–44. <https://doi.org/10.1179/174328005X14311>.
- [28] J. Røyset, N. Ryum, Kinetics and mechanisms of precipitation in an Al-0.2wt.% Sc alloy, *Materials Science and Engineering A* 396 (2005) 409–422. <https://doi.org/10.1016/j.msea.2005.02.015>.
- [29] E.A. Marquis, D.N. Seidman, M. Asta, C. Woodward, Composition evolution of nanoscale Al₃Sc precipitates in an Al-Mg-Sc alloy: Experiments and computations, *Acta Mater* 54 (2006) 119–130. <https://doi.org/10.1016/j.actamat.2005.08.035>.
- [30] R.T. Mathew, S. Singam, P. Ghosh, S.K. Masa, M.J.N.V. Prasad, The defining role of initial microstructure and processing temperature on microstructural evolution, hardness and tensile response of Al-Mg-Sc-Zr (AA5024) alloy processed by high pressure torsion, *J Alloys Compd* 901 (2022) 163548. <https://doi.org/10.1016/j.jallcom.2021.163548>.
- [31] P.H.R. Pereira, Y. Huang, M. Kawasaki, T.G. Langdon, An examination of the superplastic characteristics of Al–Mg–Sc alloys after processing, *J Mater Res* 32 (2017) 4541–4553. <https://doi.org/10.1557/jmr.2017.286>.
- [32] Y.A. Filatov, V.I. Yelagin, V. V Zakharov, New Al–Mg–Sc alloys, *Materials Science and Engineering: A* 280 (2000) 97–101. [https://doi.org/http://dx.doi.org/10.1016/S0921-5093\(99\)00673-5](https://doi.org/http://dx.doi.org/10.1016/S0921-5093(99)00673-5).
- [33] S. Komura, Z. Horita, M. Furukawa, M. Nemoto, T.G. Langdon, An evaluation of the flow behavior during high strain rate superplasticity in an Al-Mg-Sc alloy, *Metall Mater Trans A Phys Metall Mater Sci* 32 (2001) 707–716. <https://doi.org/10.1007/s11661-001-1006-9>.
- [34] F. Musin, R. Kaibyshev, Y. Motohashi, G. Itoh, Superplastic behavior and microstructure evolution in a commercial Al-Mg-Sc alloy subjected to intense plastic straining, *Metallurgical and Materials Transactions A* 35 (2004) 2383–2392. <https://doi.org/10.1007/s11661-006-0218-4>.
- [35] R. Kaibyshev, E. Avtokratova, A. Apollonov, R. Davies, High strain rate superplasticity in an Al-Mg-Sc-Zr alloy subjected to simple thermomechanical processing, *Scr Mater* 54 (2006) 2119–2124. <https://doi.org/10.1016/j.scriptamat.2006.03.020>.
- [36] E. Avtokratova, O. Sitdikov, M. Markushev, R. Mulyukov, Extraordinary high-strain rate superplasticity of severely deformed Al–Mg–Sc–Zr alloy, *Materials*

- Science and Engineering: A 538 (2012) 386–390. <https://doi.org/10.1016/j.msea.2012.01.041>.
- [37] D. Yuzbekova, A. Mogucheva, R. Kaibyshev, Superplasticity of ultrafine-grained Al–Mg–Sc–Zr alloy, *Materials Science and Engineering A* 675 (2016) 228–242. <https://doi.org/10.1016/j.msea.2016.08.074>.
- [38] G. Sakai, Z. Horita, T.G. Langdon, Grain refinement and superplasticity in an aluminum alloy processed by high-pressure torsion, *Materials Science and Engineering: A* 393 (2005) 344–351. <https://doi.org/10.1016/j.msea.2004.11.007>.
- [39] S.V. Dobatkin, V.V. Zakharov, A.Yu. Vinogradov, K. Kitagawa, N.A. Krasil'nikov, T.D. Rostova, E.N. Bastarash, Nanocrystalline structure formation in Al-Mg-Sc alloys during severe plastic deformation, *Russian Metallurgy (Metally)* 2006 (2006) 533–540. <https://doi.org/10.1134/S0036029506060115>.
- [40] Z. Horita, T.G. Langdon, Achieving exceptional superplasticity in a bulk aluminum alloy processed by high-pressure torsion, *Scr Mater* 58 (2008) 1029–1032. <https://doi.org/10.1016/j.scriptamat.2008.01.043>.
- [41] V.N. Perevezentsev, M.Yu. Shcherban', M.Yu. Murashkin, R.Z. Valiev, High-strain-rate superplasticity of nanocrystalline aluminum alloy 1570, *Technical Physics Letters* 33 (2007) 648–650. <https://doi.org/10.1134/S106378500708007X>.
- [42] Y. Harai, K. Edalati, Z. Horita, T.G. Langdon, Using ring samples to evaluate the processing characteristics in high-pressure torsion, *Acta Mater* 57 (2009) 1147–1153. <https://doi.org/10.1016/j.actamat.2008.10.046>.
- [43] M. El-Tahawy, P.H.R. Pereira, Y. Huang, H. Park, H. Choe, T.G. Langdon, J. Gubicza, Exceptionally high strength and good ductility in an ultrafine-grained 316L steel processed by severe plastic deformation and subsequent annealing, *Mater Lett* 214 (2018) 240–242. <https://doi.org/10.1016/j.matlet.2017.12.040>.
- [44] P.H.R. Pereira, Y.C. Wang, Y. Huang, T.G. Langdon, Influence of grain size on the flow properties of an Al-Mg-Sc alloy over seven orders of magnitude of strain rate, *Materials Science and Engineering A* 685 (2017) 367–376. <https://doi.org/10.1016/j.msea.2017.01.020>.
- [45] M. Kai, Z. Horita, T.G. Langdon, Developing grain refinement and superplasticity in a magnesium alloy processed by high-pressure torsion, *Materials Science and Engineering A* 488 (2008) 117–124. <https://doi.org/10.1016/j.msea.2007.12.046>.
- [46] Y. Harai, M. Kai, K. Kaneko, Z. Horita, T.G. Langdon, Microstructural and Mechanical Characteristics of AZ61 Magnesium Alloy Processed by High-Pressure Torsion, *Mater Trans* 49 (2008) 76–83. <https://doi.org/10.2320/matertrans.ME200718>.
- [47] P.H.R. Pereira, Y. Huang, T.G. Langdon, Examining the microhardness evolution and thermal stability of an Al–Mg–Sc alloy processed by high-pressure torsion at a high temperature, *Journal of Materials Research and Technology* 6 (2017) 348–354. <https://doi.org/10.1016/j.jmrt.2017.05.008>.
- [48] D.C. Machado, P.C. Alves Flausino, Y. Huang, P.R. Cetlin, T.G. Langdon, P.H.R. Pereira, Influence of processing temperature on microhardness evolution, microstructure and superplastic behaviour in an Al–Mg alloy processed by high-

- pressure torsion, *Journal of Materials Research and Technology* 24 (2023) 2850–2867. <https://doi.org/10.1016/J.JMRT.2023.03.167>.
- [49] R.B. Figueiredo, P.R. Cetlin, T.G. Langdon, Using finite element modeling to examine the flow processes in quasi-constrained high-pressure torsion, *Materials Science and Engineering A* 528 (2011) 8198–8204. <https://doi.org/10.1016/j.msea.2011.07.040>.
- [50] P.H.R. Pereira, R.B. Figueiredo, P.R. Cetlin, T.G. Langdon, Using finite element modelling to examine the flow process and temperature evolution in HPT under different constraining conditions, *IOP Conf Ser Mater Sci Eng* 63 (2014) 012041. <https://doi.org/10.1088/1757-899X/63/1/012041>.
- [51] R.B. Figueiredo, P.H.R. Pereira, M.T.P. Aguilar, P.R. Cetlin, T.G. Langdon, Using finite element modeling to examine the temperature distribution in quasi-constrained high-pressure torsion, *Acta Mater* 60 (2012) 3190–3198. <https://doi.org/10.1016/j.actamat.2012.02.027>.
- [52] M. Kawasaki, T.G. Langdon, The significance of strain reversals during processing by high-pressure torsion, *Materials Science and Engineering A* 498 (2008) 341–348. <https://doi.org/10.1016/j.msea.2008.08.021>.
- [53] A. Loucif, R.B. Figueiredo, M. Kawasaki, T. Baudin, F. Brisset, R. Chemam, T.G. Langdon, Effect of aging on microstructural development in an Al-Mg-Si alloy processed by high-pressure torsion, *J Mater Sci* 47 (2012) 7815–1820. <https://doi.org/10.1007/s10853-012-6400-8>.
- [54] H. Shahmir, P.H.R. Pereira, Y. Huang, T.G. Langdon, Mechanical properties and microstructural evolution of nanocrystalline titanium at elevated temperatures, *Materials Science and Engineering: A* 669 (2016) 358–366. <https://doi.org/10.1016/j.msea.2016.05.105>.
- [55] Y. Huang, M. Lemang, N.X. Zhang, P.H.R. Pereira, T.G. Langdon, Achieving superior grain refinement and mechanical properties in vanadium through high-pressure torsion and subsequent short-term annealing, *Materials Science and Engineering A* 655 (2016) 60–69. <https://doi.org/10.1016/j.msea.2015.12.086>.
- [56] P.H.R. Pereira, R.B. Figueiredo, P.R. Cetlin, T.G. Langdon, An examination of the elastic distortions of anvils in high-pressure torsion, *Materials Science and Engineering A* 631 (2015) 201–208. <https://doi.org/10.1016/j.msea.2015.02.052>.
- [57] P.H.R. Pereira, Y. Huang, T.G. Langdon, Examining the thermal stability of an Al-Mg-Sc alloy processed by high-pressure torsion, *Materials Research* 20 (2017) 39–45. <https://doi.org/http://dx.doi.org/10.1590/1980-5373-MR-2017-0207>.
- [58] Y. Huang, P. Bazarnik, D. Wan, D. Luo, P.H.R. Pereira, M. Lewandowska, J. Yao, B.E. Hayden, T.G. Langdon, The fabrication of graphene-reinforced Al-based nanocomposites using high-pressure torsion, *Acta Mater* 164 (2019) 499–511.
- [59] T.G. Langdon, Seventy-five years of superplasticity: Historic developments and new opportunities, *J Mater Sci* 44 (2009) 5998–6010. <https://doi.org/10.1007/s10853-009-3780-5>.

- [60] K. Higashi, M. Mabuchi, T.G. Langdon, High-Strain-Rate Superplasticity in Metallic Materials and the Potential for Ceramic Materials., *ISIJ International* 36 (1996) 1423–1438. <https://doi.org/10.2355/isijinternational.36.1423>.
- [61] T.G. Langdon, Fracture processes in superplastic flow, *Metal Science* 16 (1982) 175–183. <https://doi.org/10.1179/030634582790427208>.
- [62] M. Kawasaki, T.G. Langdon, Review: achieving superplasticity in metals processed by high-pressure torsion, *J Mater Sci* 49 (2014) 6487–6496. <https://doi.org/10.1007/s10853-014-8204-5>.
- [63] M. Kawasaki, T.G. Langdon, Developing superplasticity and a deformation mechanism map for the Zn-Al eutectoid alloy processed by high-pressure torsion, *Materials Science and Engineering A* 528 (2011) 6140–6145. <https://doi.org/10.1016/j.msea.2011.04.053>.
- [64] J.K. Mackenzie, Second paper on statistics associated with the random disorientation of cubes, *Biometrika* 45 (1958) 229–240. <https://doi.org/10.2307/2333059>.
- [65] T.G. Langdon, An evaluation of the strain contributed by grain boundary sliding in superplasticity, *Materials Science and Engineering, A* 174 (1994) 225–230. [https://doi.org/https://doi.org/10.1016/0921-5093\(94\)91092-8](https://doi.org/https://doi.org/10.1016/0921-5093(94)91092-8).
- [66] R.B. Figueiredo, P.H.R. Pereira, T.G. Langdon, Effect of Numbers of Turns of High-Pressure Torsion on the Development of Exceptional Ductility in Pure Magnesium, *Adv Eng Mater* 22 (2020) 1900565. <https://doi.org/10.1002/adem.201900565>.
- [67] M. Kawasaki, T.G. Langdon, Principles of superplasticity in ultrafine-grained materials, *J Mater Sci* 42 (2007) 1782–1796. <https://doi.org/10.1007/s10853-006-0954-2>.
- [68] F.A. Mohamed, Creep and Superplasticity: Evolution and Rationalization, *Adv Eng Mater* 22 (2020) 1900532. <https://doi.org/10.1002/ADEM.201900532>.
- [69] F.A. Mohamed, M.M.I. Ahmed, T.G. Langdon, Factors influencing ductility in the superplastic Zn-22 Pct Al eutectoid, *Metallurgical Transactions A* 8 (1977) 933–938. <https://doi.org/10.1007/BF02661575>.
- [70] H. Ishikawa, F.A. Mohamed, T.G. Langdon, The influence of strain rate on ductility in the superplastic Zn–22% Al eutectoid, *Philosophical Magazine* 32 (1975) 1269–1271. <https://doi.org/10.1080/14786437508228105>.
- [71] F.J. Humphreys, M. Hatherly, *Recrystallization and Related Annealing Phenomena*, Second edition, Pergamon Press, Oxford, 2004. <https://doi.org/10.1016/B978-0-08-044164-1.X5000-2>.
- [72] F.J. Humphreys, A unified theory of recovery, recrystallization and grain growth, based on the stability and growth of cellular microstructures - II. The effect of second-phase particles, *Acta Mater* 45 (1997) 5031–5039. [https://doi.org/10.1016/S1359-6454\(97\)00173-0](https://doi.org/10.1016/S1359-6454(97)00173-0).
- [73] C.A. Bronkhorst, S.R. Kalidindi, L. Anand, Polycrystalline Plasticity and the Evolution of Crystallographic Texture in FCC Metals, *Philosophical Transactions*

- of the Royal Society A 341 (1992) 443–477.
<https://doi.org/10.1098/rsta.1992.0111>.
- [74] W.A. Rachinger, Relative Grain Translations in the Plastic flow of Aluminium, *Journal of the Institute of Metals* 81 (1952) 33–41.
- [75] T.G. Langdon, Identifying creep mechanisms in plastic flow, *Zeitschrift Fuer Metallkunde* 96 (2005) 522–531. <https://doi.org/10.3139/146.101066>.
- [76] G. Rai, N.J. Grant, On the measurements of superplasticity in an Al-Cu alloy, *Metallurgical Transactions A* 6 (1975) 385–390.
<https://doi.org/10.1007/BF02667294>.
- [77] T.G. Langdon, The mechanical properties of superplastic materials, *Metallurgical Transactions A* 13 (1982) 689–701. <https://doi.org/10.1007/BF02642383>.
- [78] F.A. Mohamed, T.G. Langdon, Creep at low stress levels in the superplastic Zn-22% Al eutectoid, *Acta Metallurgica* 23 (1975) 117–124.
[https://doi.org/10.1016/0001-6160\(75\)90076-0](https://doi.org/10.1016/0001-6160(75)90076-0).
- [79] M. Kawasaki, N. Balasubramanian, T.G. Langdon, Flow mechanisms in ultrafine-grained metals with an emphasis on superplasticity, *Materials Science and Engineering: A* 528 (2011) 6624–6629.
<https://doi.org/10.1016/j.msea.2011.05.005>.
- [80] M. Kawasaki, T.G. Langdon, Review: achieving superplastic properties in ultrafine-grained materials at high temperatures, *J Mater Sci* 51 (2016) 19–32.
<https://doi.org/10.1007/s10853-015-9176-9>.
- [81] F.A. Mohamed, T.G. Langdon, Deformation mechanism maps based on grain size, *Metallurgical Transactions* 5 (1974) 2339–2345.
<https://doi.org/10.1007/BF02644014>.
- [82] R.B. Figueiredo, S. Terzi, T.G. Langdon, Using X-ray microtomography to evaluate cavity formation in a superplastic magnesium alloy processed by equal-channel angular pressing, *Acta Mater* 58 (2010) 5737–5748.
<https://doi.org/10.1016/j.actamat.2010.06.049>.
- [83] J.E. Bird, A.K. Mukherjee, J.E. Dorn, D.G. Brandon, A. Rosen (Eds.), *Quantitative Relation between Properties and Microstructure*, Israel Universities Press, Jerusalem, Israel, (1969) 255–342.
- [84] R. Kapoor, J.B. Singh, J.K. Chakravarty, High strain rate behavior of ultrafine-grained Al-1.5 Mg, *Materials Science and Engineering A* 496 (2008) 308–315.
<https://doi.org/10.1016/j.msea.2008.05.043>.
- [85] R.B. Figueiredo, M. Kawasaki, T.G. Langdon, Seventy years of Hall-Petch, ninety years of superplasticity and a generalized approach to the effect of grain size on flow stress, *Prog Mater Sci* 137 (2023) 101131.
<https://doi.org/10.1016/J.PMATSCI.2023.101131>.
- [86] R.B. Figueiredo, T.G. Langdon, Deformation mechanisms in ultrafine-grained metals with an emphasis on the Hall-Petch relationship and strain rate sensitivity, *Journal of Materials Research and Technology* 14 (2021) 137.
<https://doi.org/10.1016/j.jmrt.2021.06.016>.

- [87] Y.H. Zhao, Y.Z. Guo, Q. Wei, A.M. Dangelewicz, C. Xu, Y.T. Zhu, T.G. Langdon, Y.Z. Zhou, E.J. Lavernia, Influence of specimen dimensions on the tensile behavior of ultrafine-grained Cu, *Scr Mater* 59 (2008) 627–630. <https://doi.org/10.1016/j.scriptamat.2008.05.031>.
- [88] Y.H. Zhao, Y.Z. Guo, Q. Wei, T.D. Topping, A.M. Dangelewicz, Y.T. Zhu, T.G. Langdon, E.J. Lavernia, Influence of specimen dimensions and strain measurement methods on tensile stress–strain curves, *Materials Science and Engineering: A* 525 (2009) 68–77. <https://doi.org/10.1016/j.msea.2009.06.031>.
- [89] N.T.C. Nguyen, P. Asghari-Rad, P. Sathiyamoorthi, A. Zargaran, C.S. Lee, H.S. Kim, Ultrahigh high-strain-rate superplasticity in a nanostructured high-entropy alloy, *Nat Commun* 11 (2020) 2736. <https://doi.org/10.1038/s41467-020-16601-1>.
- [90] C.T. Wang, Z. Li, J.T. Wang, T.G. Langdon, New developments in the processing of metallic alloys for achieving exceptional superplastic properties, *Materials Research Proceedings* 32 (2023) 3–14. <https://doi.org/10.21741/97816449025615-1>.
- [91] C.T. Wang, Z. Li, Y. He, J.T. Wang, T.G. Langdon, Microstructural Evolution and Tensile Testing of a Bi–Sn (57/43) Alloy Processed by Tube High-Pressure Shearing, *Crystals (Basel)* 11 (2021) 1229. <https://doi.org/10.3390/cryst11101229>.
- [92] J.T. Wang, Z. Li, J. Wang, T.G. Langdon, Principles of severe plastic deformation using tube high-pressure shearing, *Scr Mater* 67 (2012) 810–813. <https://doi.org/10.1016/j.scriptamat.2012.07.028>.
- [93] G. Sakai, K. Nakamura, Z. Horita, T.G. Langdon, Developing high-pressure torsion for use with bulk samples, *Materials Science and Engineering A* 406 (2005) 268–273. <https://doi.org/10.1016/j.msea.2005.06.049>.
- [94] S. Komura, M. Furukawa, Z. Horita, M. Nemoto, T.G. Langdon, Optimizing the procedure of equal-channel angular pressing for maximum superplasticity, *Materials Science and Engineering A* 297 (2001) 111–118. [https://doi.org/10.1016/S0921-5093\(00\)01255-7](https://doi.org/10.1016/S0921-5093(00)01255-7).
- [95] P. Ghosh, O. Renk, R. Pippan, Microtexture analysis of restoration mechanisms during high pressure torsion of pure nickel, *Materials Science and Engineering A* 684 (2017) 101–109. <https://doi.org/10.1016/j.msea.2016.12.032>.
- [96] O. Renk, R. Pippan, Transition from thermally assisted to mechanically driven boundary migration and related apparent activation energies, *Scr Mater* 154 (2018) 212–215. <https://doi.org/10.1016/j.scriptamat.2018.05.052>.
- [97] O. Renk, R. Pippan, Saturation of Grain Refinement during Severe Plastic Deformation of Single Phase Materials: Reconsiderations, Current Status and Open Questions, *Mater.Trans.* 60 (2019) 1270–1282. <https://doi.org/10.2320/matertrans.MF201918>.

Figure captions:

Fig. 1. Colour-coded contour maps revealing the distributions of the Vickers microhardness over the surfaces of Al-Mg-Sc discs processed by 10 HPT revolutions at (a) 300 and (b) 450 K.

Fig. 2. STEM images showing dislocation and grain structures in the Al-3Mg-0.2Sc alloy processed through 10 turns of HPT at (a and b) RT and (c and d) 450 K.

Fig. 3. True stress vs true strain curves for the Al-3Mg-0.2Sc alloy processed through 10 HPT turns at either 300 or 450 K and then tensile tested at (a, c) 523 and (b, d) 673 K using strain rates from 3.3×10^{-4} to 1.4 s^{-1} .

Fig. 4. Fractured specimens of the Al-3Mg-0.2Sc alloy processed by 10 HPT turns at (a) 300 K and (b) 450 K and then pulled to failure at 523 and 673 K.

Fig. 5. Elongation vs strain rate for the Al-3Mg-0.2Sc alloy processed by 10 HPT revolutions at (a) 300 and (b) 450 K and tensile tested using various strain rates at temperatures from 473 to 723 K.

Fig. 6. True stress at $\epsilon = 0.3$ vs strain rate for the Al-3Mg-0.2Sc alloy processed by 10 HPT revolutions at (a) 300 and (b) 450 K and tensile tested using various strain rates at temperatures from 473 to 723 K.

Fig. 7. Orientation maps and corresponding $\{111\}$ pole figures taken along (a) the undeformed and (b) the gauge area of the fractured specimens of the Al-3Mg-0.2Sc alloy subjected to 10 HPT turns at 300 K and tested in tension at 673 K.

Fig. 8. Orientation maps and corresponding $\{111\}$ pole figures taken along (a, c, e) the undeformed and (b, d, f) the gauge area of the fractured specimens of the Al-3Mg-0.2Sc alloy subjected to 10 HPT revolutions at 450 K and tested in tension at 673 K at strain rates of (a, b) 1.0, (c, d) 3.3×10^{-2} and (e, f) $3.3 \times 10^{-4} \text{ s}^{-1}$.

Fig. 9. Average grain size (\bar{L}) vs total time at the testing temperature for miniature specimens of the Al-3Mg-0.2Sc alloy subjected to 10 HPT turns at (a) 300 and (b) 450 K and tested in tension at temperatures from 473 to 723 K using strain rates ranging from 3.3×10^{-4} to 1.0 s^{-1} .

Fig. 10. TEM images taken along the gauge areas of the fractured specimens of the Al-3Mg-0.2Sc alloy subjected to 10 HPT turns at (a, b) 300 and (c, d) 450 K and tested in tension at 673 K using similar strain rates.

Fig. 11. Colour-coded contour maps showing the tensile elongations achieved in miniature specimens of the Al-3Mg-0.2Sc alloy processed through 10 HPT turns at (a) 300 and (b) 450 K and tested in tension at temperatures from 473 to 723 K using strain rates ranging from 3.3×10^{-4} to 1.0 s^{-1} .

Fig. 12. Temperature and grain size compensated strain rate as a function of normalized stress for Al-3Mg-0.2Sc specimens exhibiting superplastic elongations after 10 turns of

HPT processing at 300 or 450 K and tensile tested at temperatures from 473 to 723 K: additional data are also included for various superplastic Al-Mg-Sc alloys processed by HPT [38,41,42] and the solid line shows the theoretical prediction for superplastic flow, $\dot{\epsilon}_{sp}$ [16].

Fig. 13. Plots of grain size *vs* normalized stress for the Al-3Mg-0.2Sc alloy processed by 10 HPT turns at (a) 300 and (b) 450 K and tested in tension at temperatures from 473 to 723 K using various strain rates: the solid line represents the theoretical prediction for the equilibrium subgrain size, λ [44,83,84].

Figures:

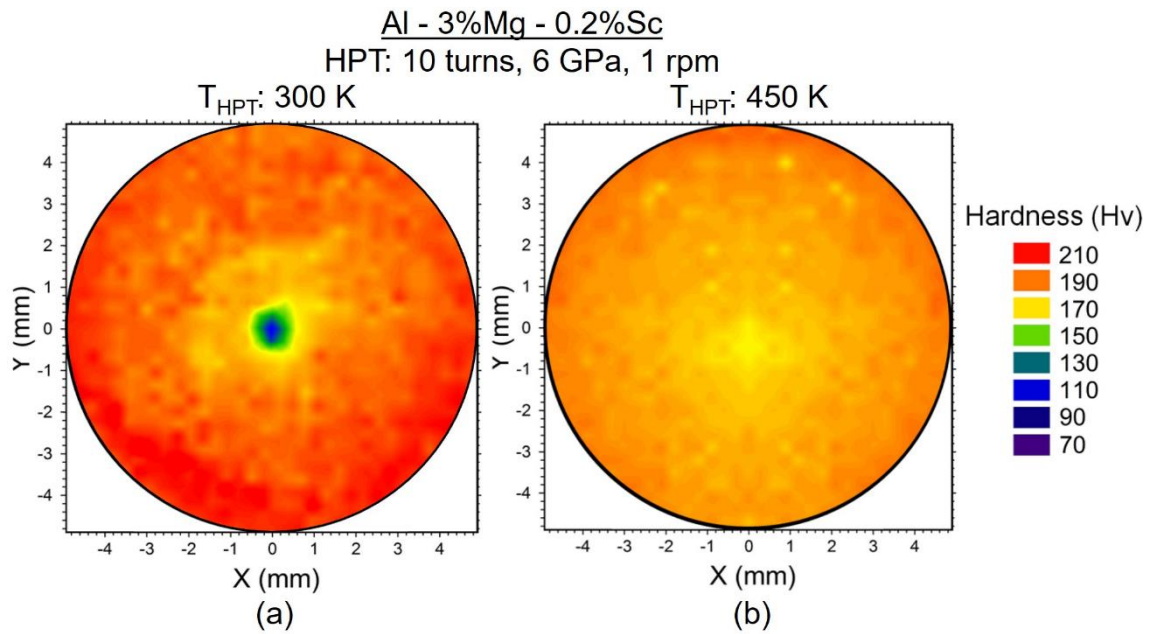


Fig. 1. Colour-coded contour maps revealing the distributions of the Vickers microhardness over the surfaces of Al-Mg-Sc discs processed by 10 HPT revolutions at (a) 300 and (b) 450 K.

Al - 3%Mg - 0.2%Sc
HPT: 10 turns, 6 GPa, 1 rpm

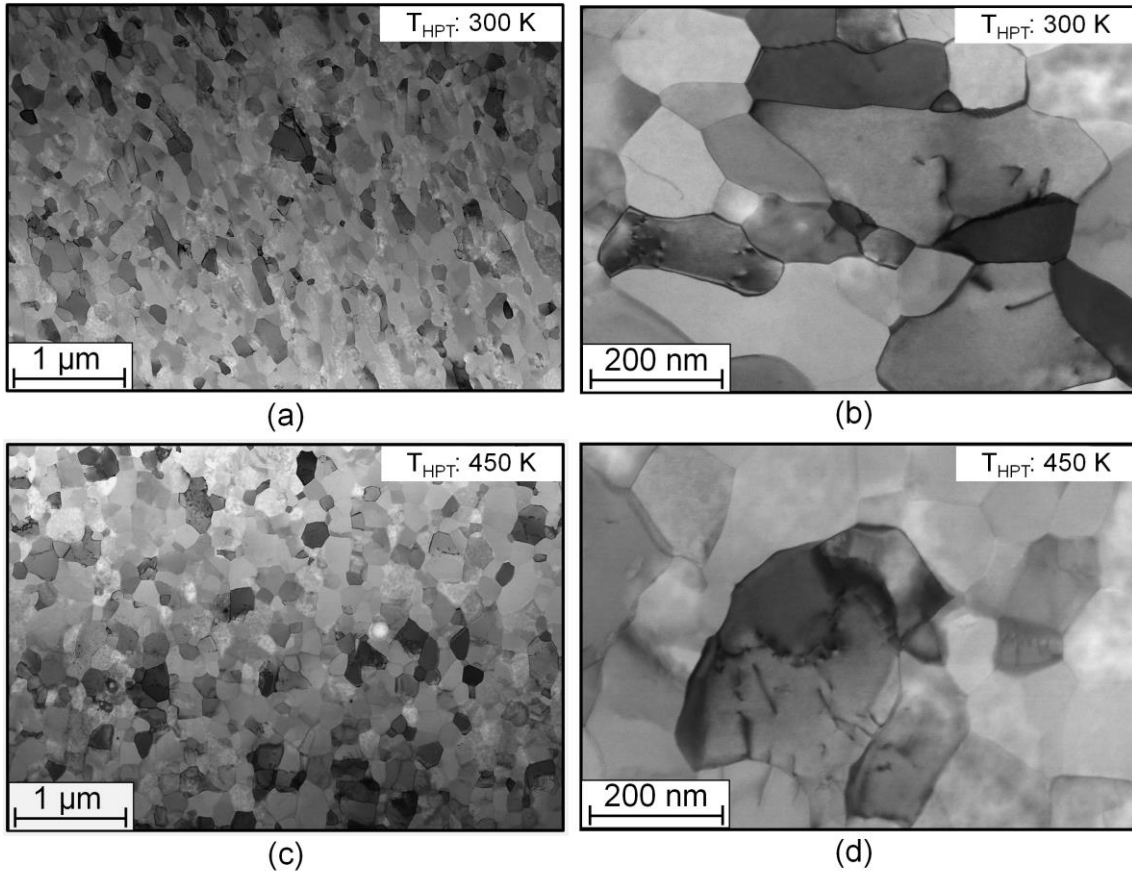


Fig. 2. STEM images showing dislocation and grain structures in the Al-3Mg-0.2Sc alloy processed through 10 turns of HPT at (a and b) RT and (c and d) 450 K.

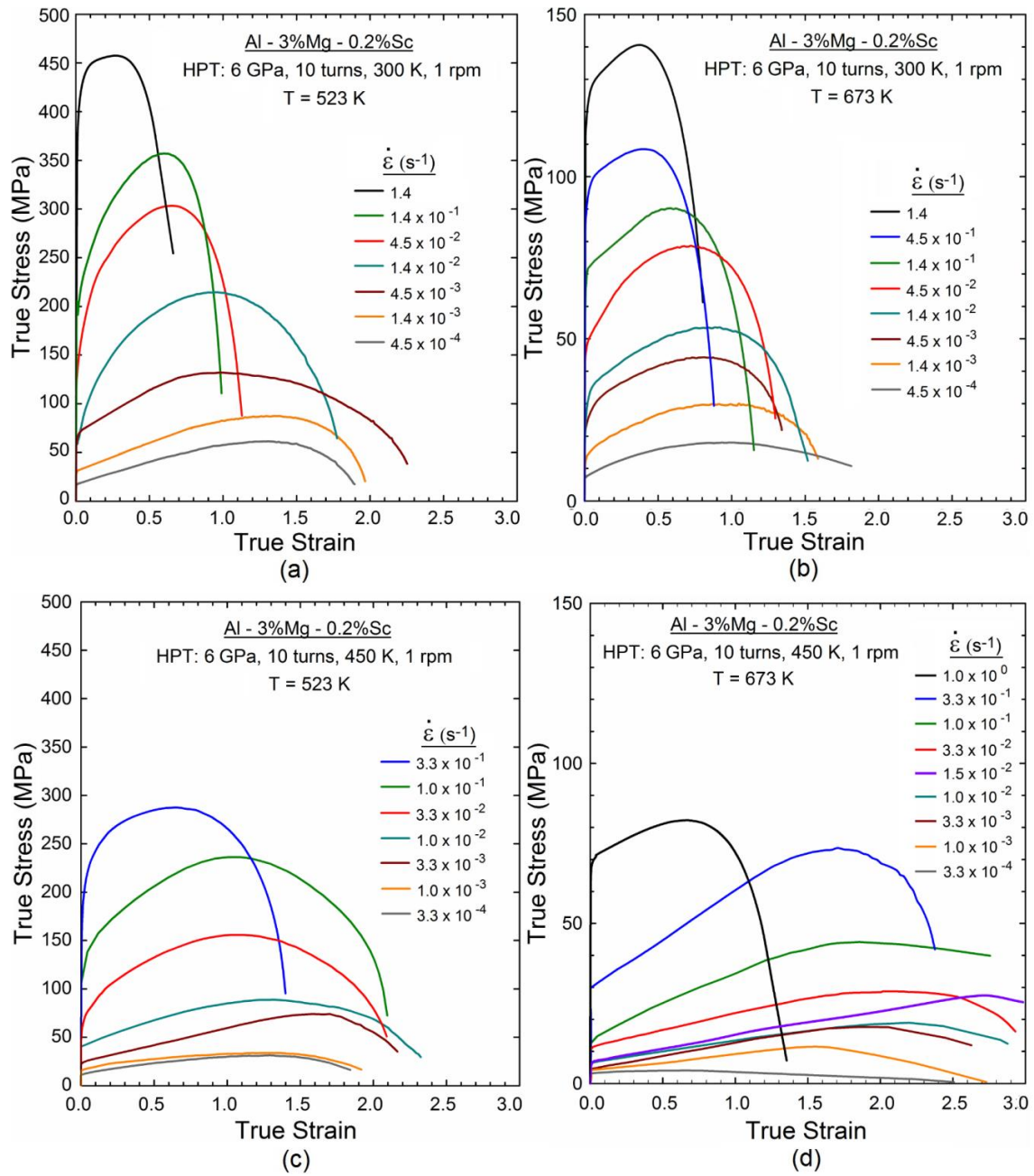
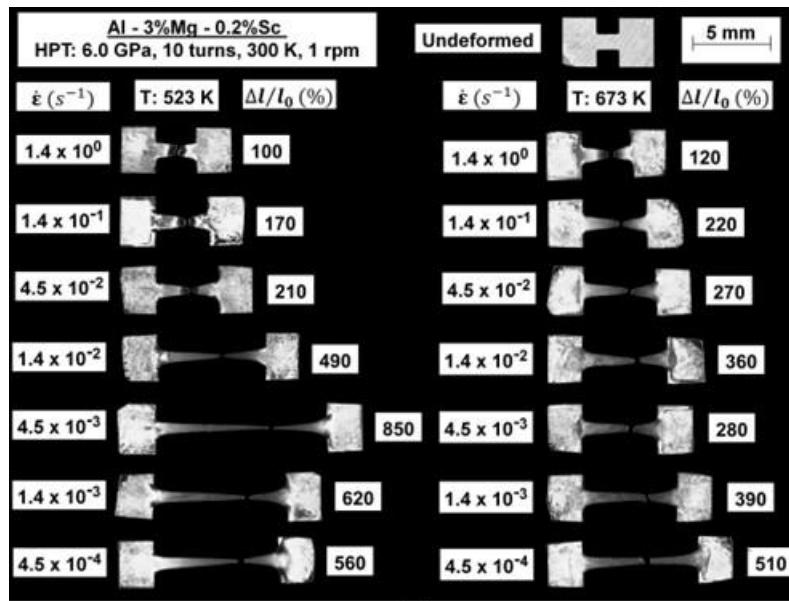
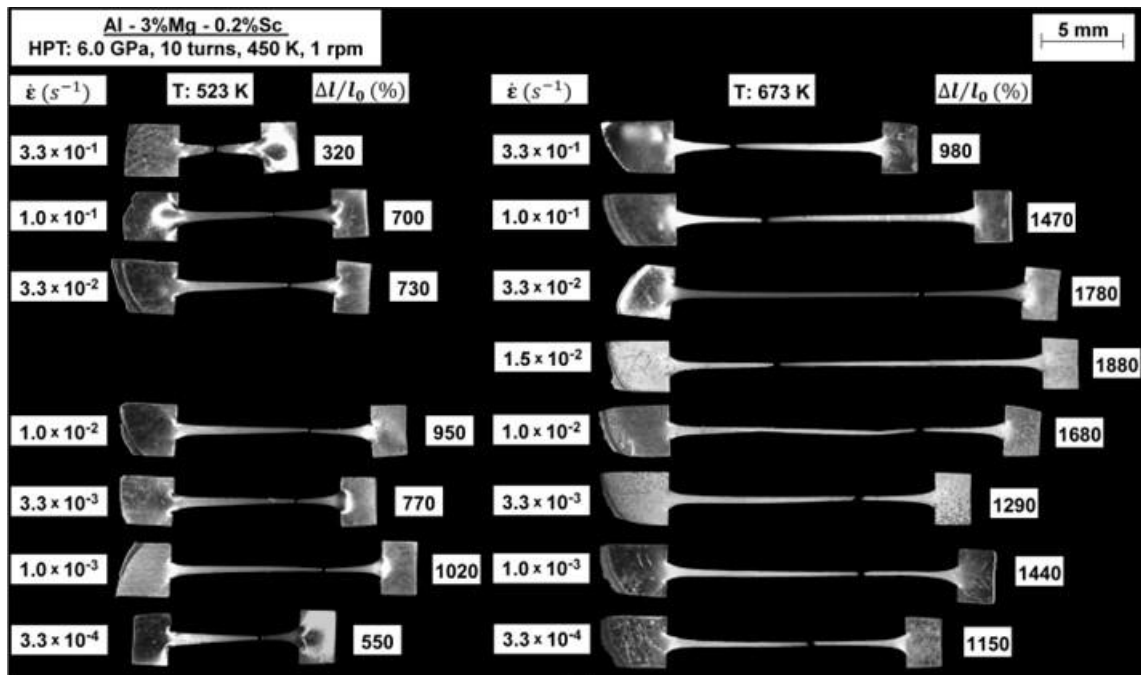


Fig. 3. True stress vs true strain curves for the Al-3Mg-0.2Sc alloy processed through 10 HPT turns at either 300 or 450 K and then tensile tested at (a, c) 523 and (b, d) 673 K using strain rates from 3.3×10^{-4} to $1.4 s^{-1}$.



(a)



(b)

Fig. 4. Fractured specimens of the Al-3Mg-0.2Sc alloy processed by 10 HPT turns at (a)

300 K and (b) 450 K and then pulled to failure at 523 and 673 K.

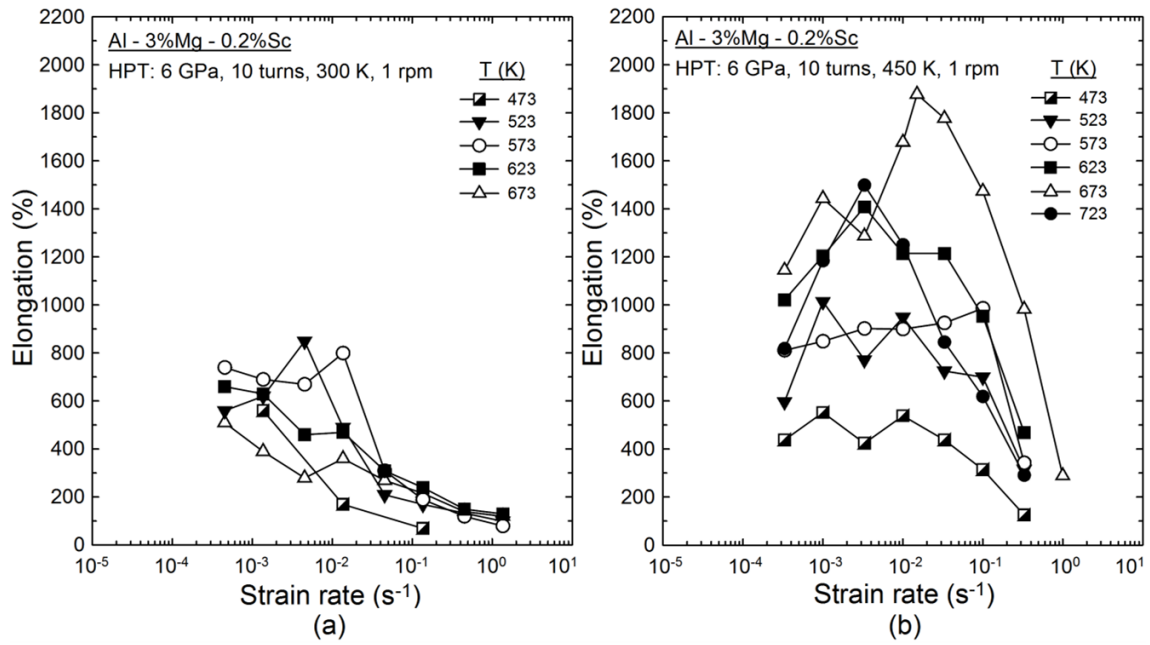


Fig. 5. Elongation vs strain rate for the Al-3Mg-0.2Sc alloy processed by 10 HPT revolutions at (a) 300 and (b) 450 K and tensile tested using various strain rates at temperatures from 473 to 723 K.

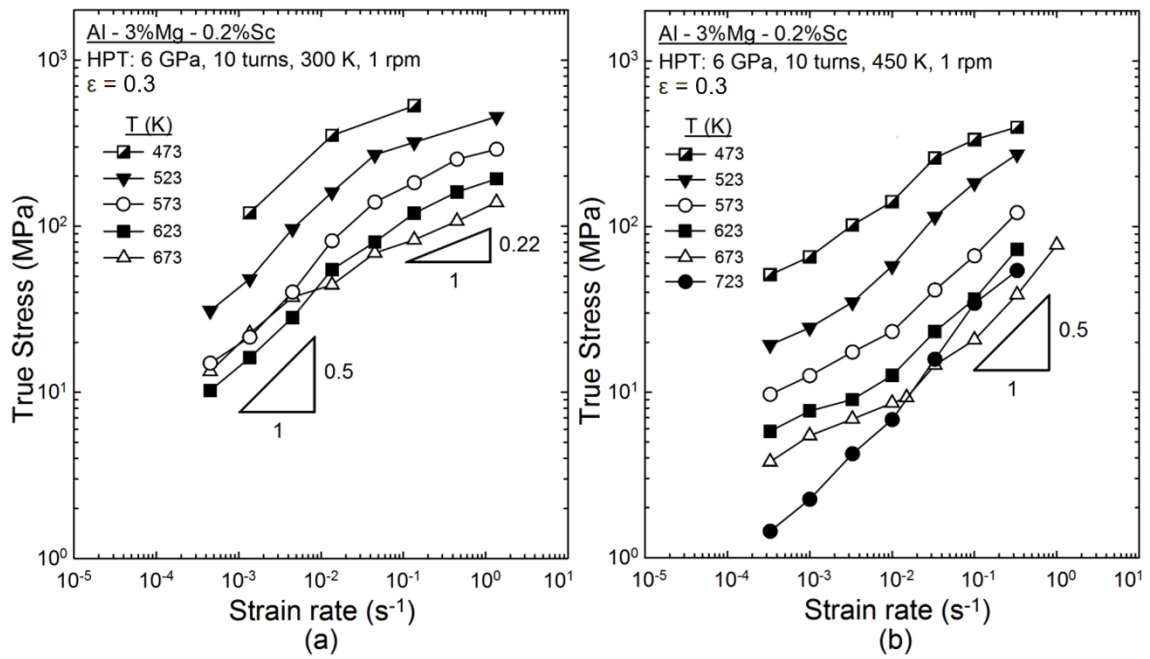


Fig. 6. True stress at $\epsilon = 0.3$ vs strain rate for the Al-3Mg-0.2Sc alloy processed by 10 HPT revolutions at (a) 300 and (b) 450 K and tensile tested using various strain rates at temperatures from 473 to 723 K.

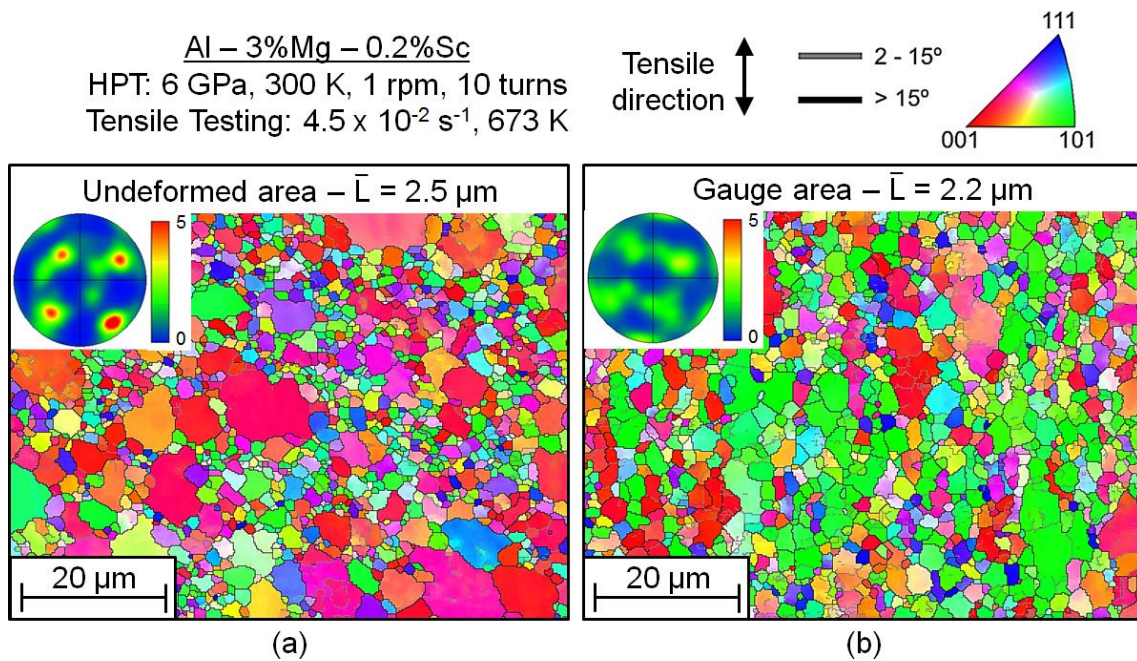


Fig. 7. Orientation maps and corresponding $\{111\}$ pole figures taken along (a) the undeformed and (b) the gauge area of the fractured specimens of the Al-3Mg-0.2Sc alloy subjected to 10 HPT turns at 300 K and tested in tension at 673 K.

Al – 3%Mg – 0.2%Sc
HPT: 6 GPa, 450 K, 1 rpm, 10 turns
Tensile Testing: 673 K

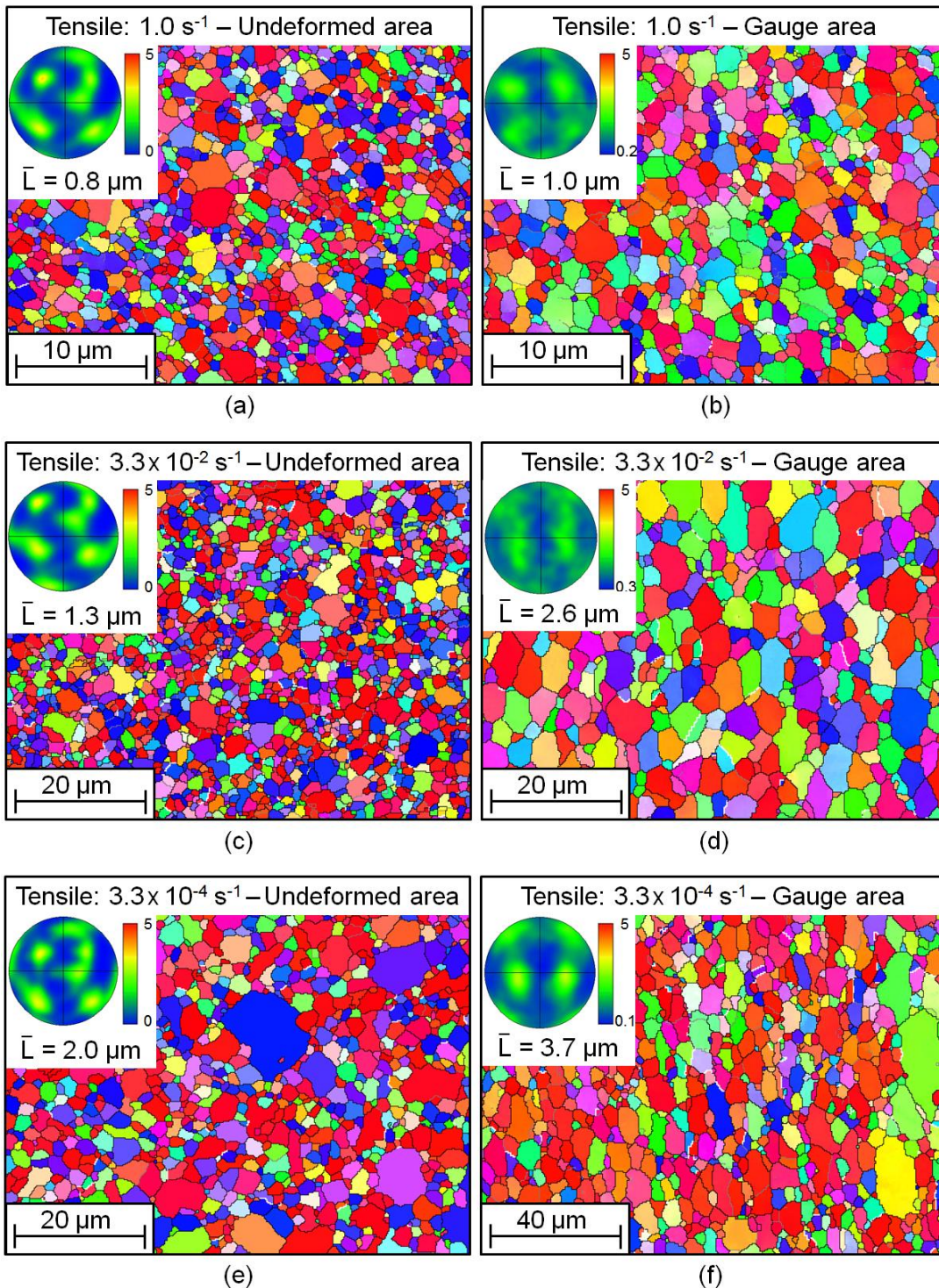
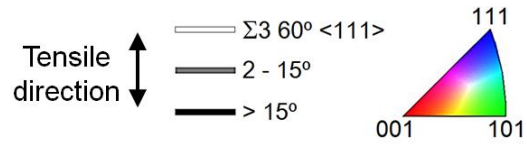


Fig. 8. Orientation maps and corresponding $\{111\}$ pole figures taken along (a, c, e) the undeformed and (b, d, f) the gauge area of the fractured specimens of the Al-3Mg-0.2Sc alloy subjected to 10 HPT revolutions at 450 K and tested in tension at 673 K at strain rates of (a, b) 1.0, (c, d) 3.3×10^{-2} and (e, f) $3.3 \times 10^{-4} \text{ s}^{-1}$.

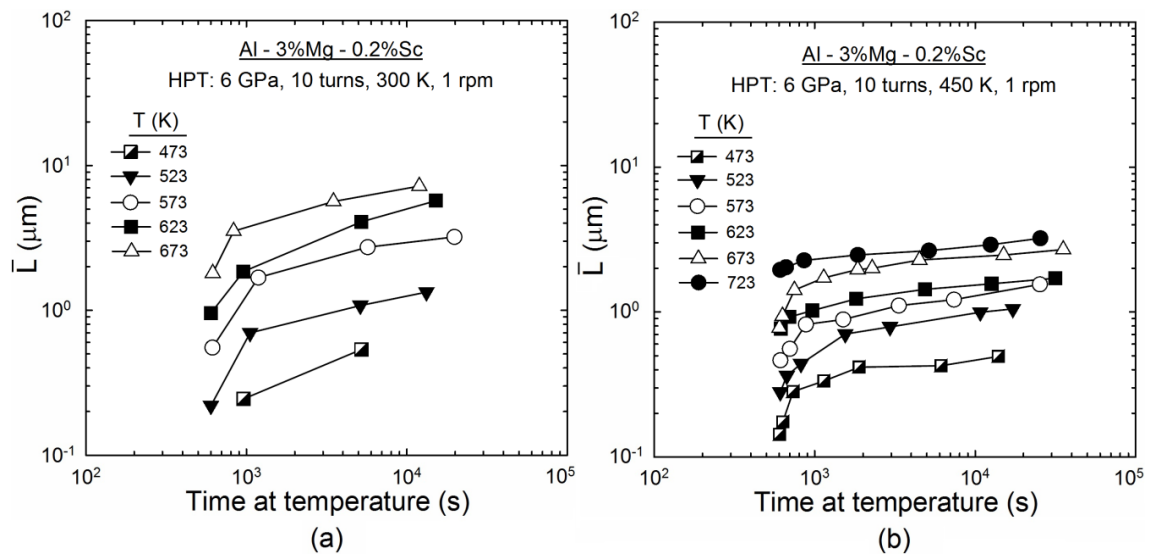


Fig. 9. Average grain size (\bar{L}) vs total time at the testing temperature for miniature specimens of the Al-3Mg-0.2Sc alloy subjected to 10 HPT turns at (a) 300 and (b) 450 K and tested in tension at temperatures from 473 to 723 K using strain rates ranging from 3.3×10^{-4} to 1.0 s^{-1} .

Al - 3%Mg - 0.2%Sc
HPT: 10 turns, 6 GPa, 1 rpm

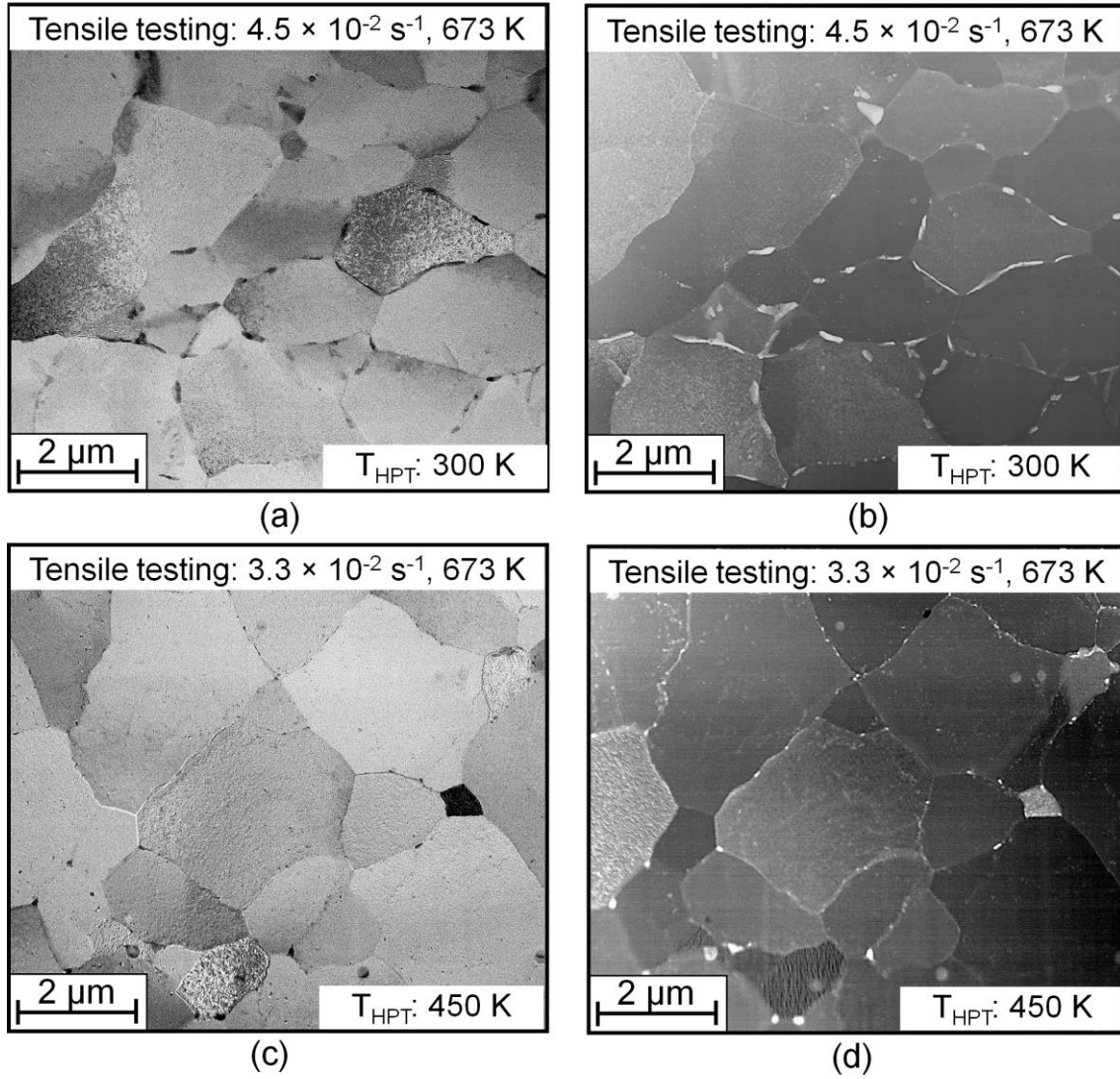


Fig. 10. TEM images taken along the gauge areas of the fractured specimens of the Al-3Mg-0.2Sc alloy subjected to 10 HPT turns at (a, b) 300 and (c, d) 450 K and tested in tension at 673 K using similar strain rates.

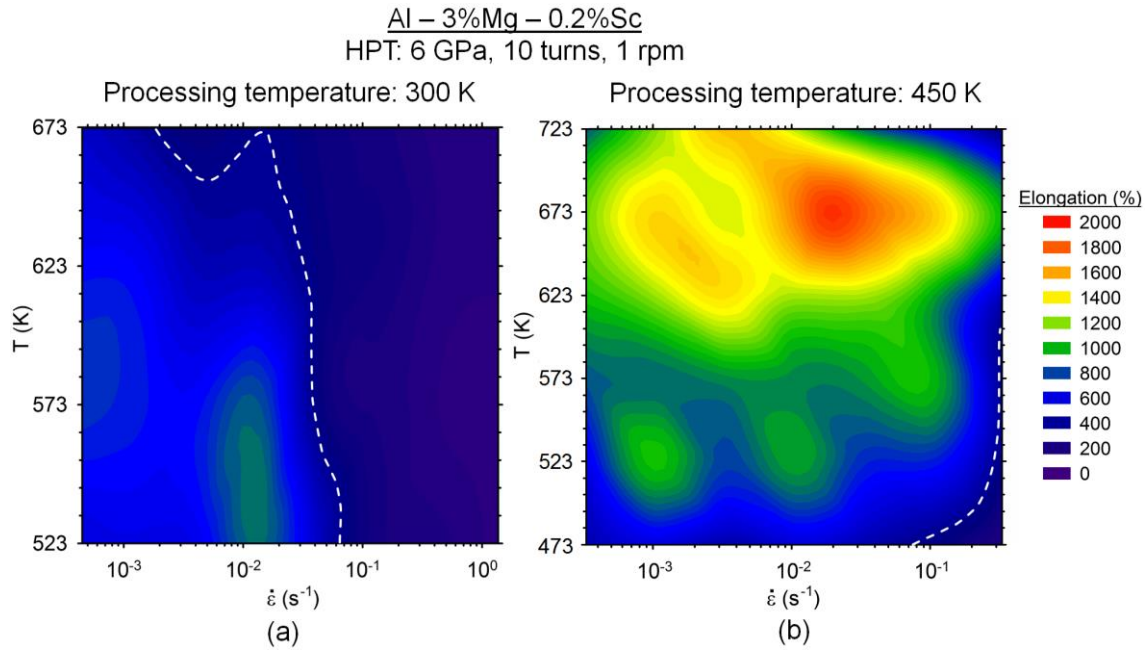


Fig. 11. Colour-coded contour maps showing the tensile elongations achieved in miniature specimens of the Al-3Mg-0.2Sc alloy processed through 10 HPT turns at (a) 300 and (b) 450 K and tested in tension at temperatures from 473 to 723 K using strain rates ranging from 3.3×10^{-4} to 1.0 s^{-1} .

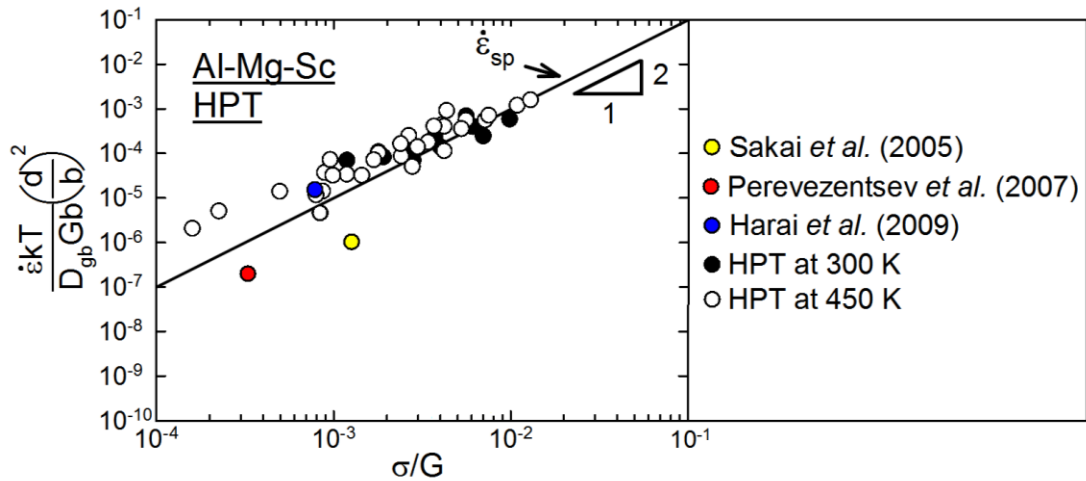


Fig. 12. Temperature and grain size compensated strain rate as a function of normalized stress for Al-3Mg-0.2Sc specimens exhibiting superplastic elongations after 10 turns of HPT processing at 300 or 450 K and tensile tested at temperatures from 473 to 723 K: additional data are also included for various superplastic Al-Mg-Sc alloys processed by HPT [38,41,42] and the solid line shows the theoretical prediction for superplastic flow,

$$\dot{\epsilon}_{sp} [16].$$

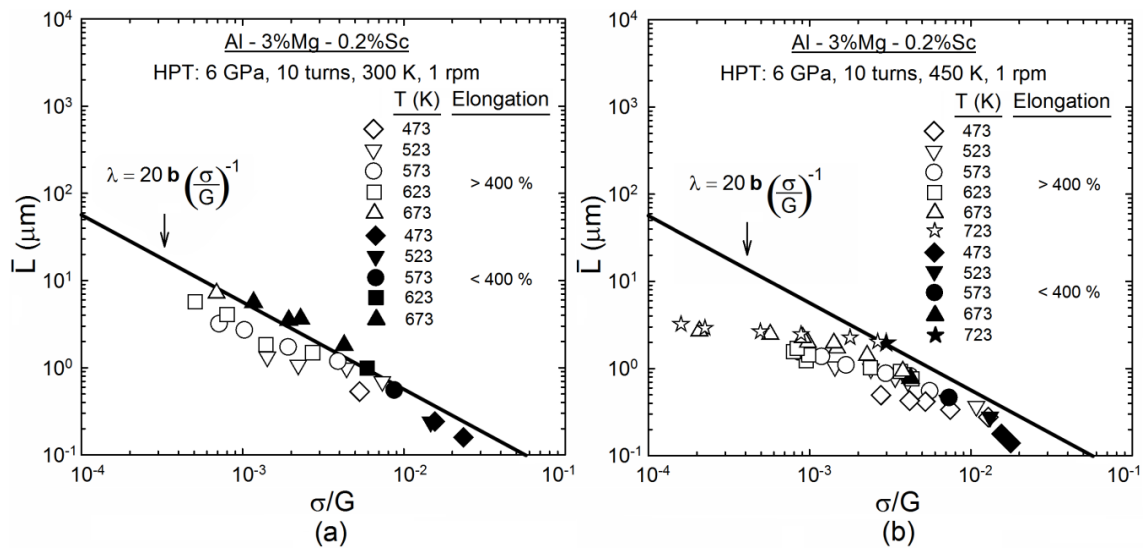


Fig. 13. Plots of grain size vs normalized stress for the Al-3Mg-0.2Sc alloy processed by 10 HPT turns at (a) 300 and (b) 450 K and tested in tension at temperatures from 473 to 723 K using various strain rates: the solid line represents the theoretical prediction for the equilibrium subgrain size, λ [44,83,84].

Supplementary Material:

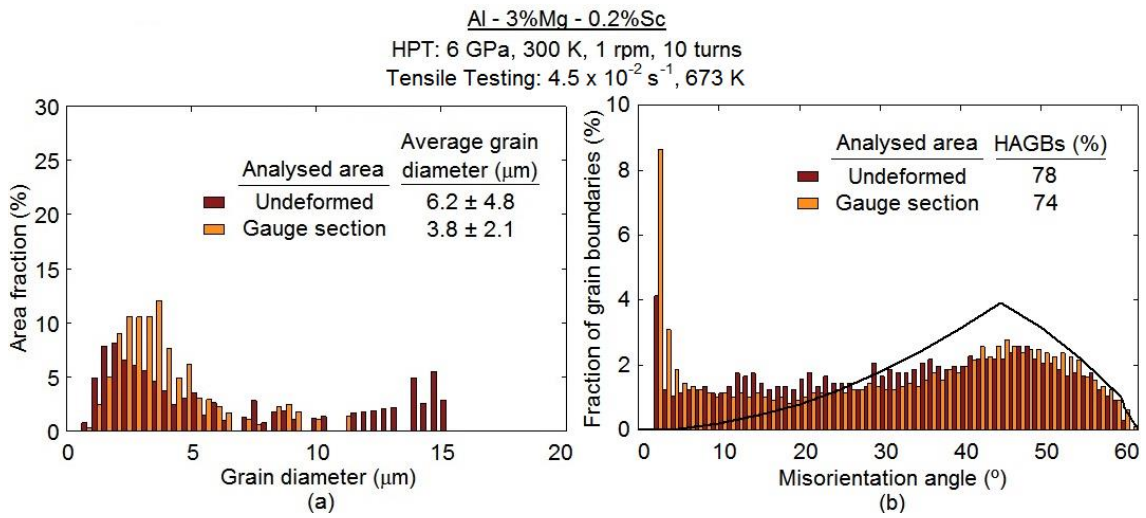


Fig. 1A. Histograms of (a) the area fraction of grain diameters and (b) of the fraction of grain boundaries as a function of misorientation angle for the Al-3Mg-0.2Sc alloy processed through 10 HPT turns at 300 K and further tested in tension at 673 K.

Al - 3%Mg - 0.2%Sc
HPT: 6 GPa, 450 K, 1 rpm, 10 turns
Tensile Testing: 673 K

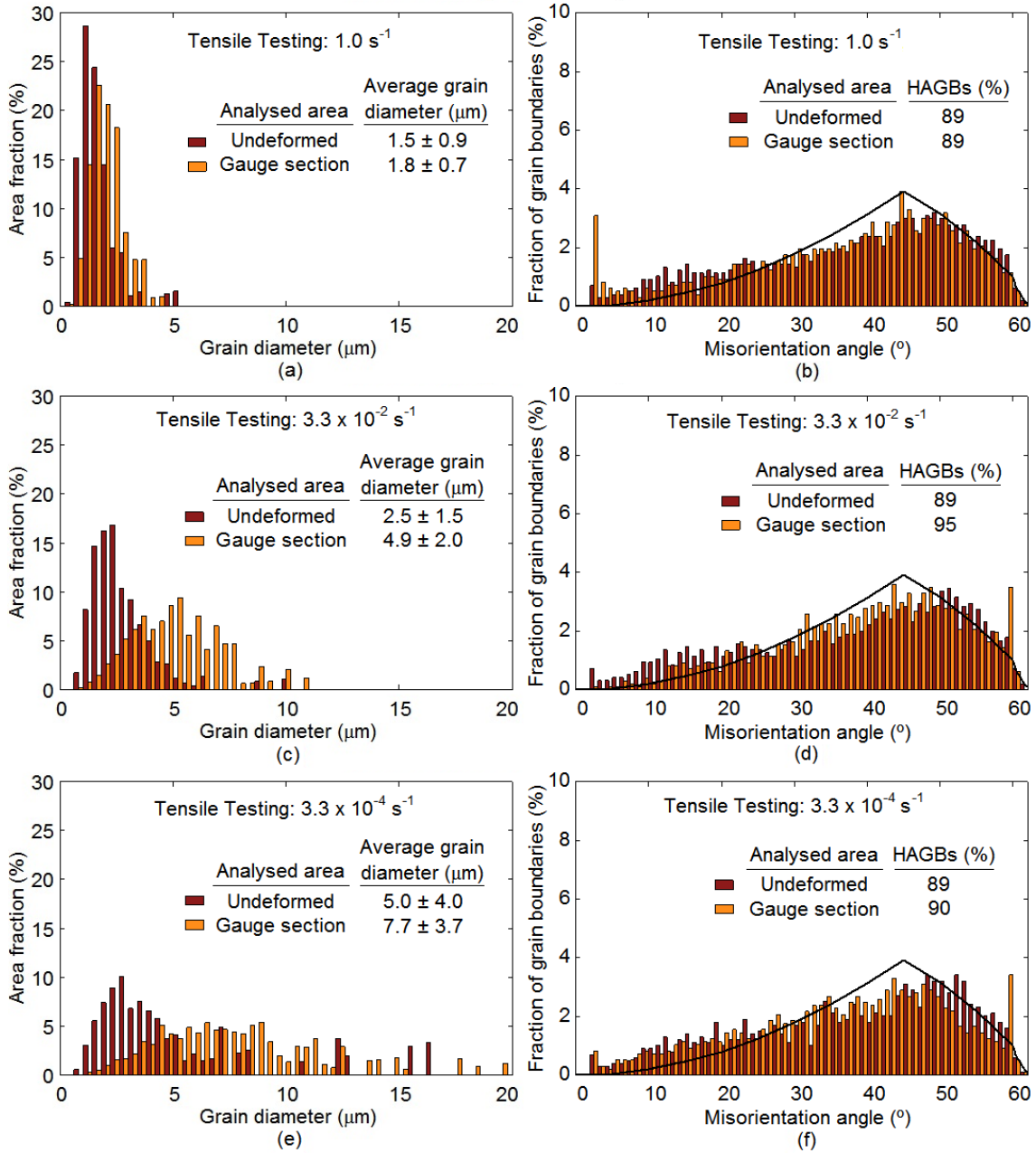


Fig. 2A. Histograms of (a, c, e) the area fraction of grain diameters and (b, d, f) of the fraction of grain boundaries as a function of misorientation angle for the Al-3Mg-0.2Sc alloy processed through 10 HPT turns at 450 K and further tested in tension at 673 K at strain rates of (a, b) 1.0, (c, d) 3.3×10^{-2} and (e, f) $3.3 \times 10^{-4} \text{ s}^{-1}$.

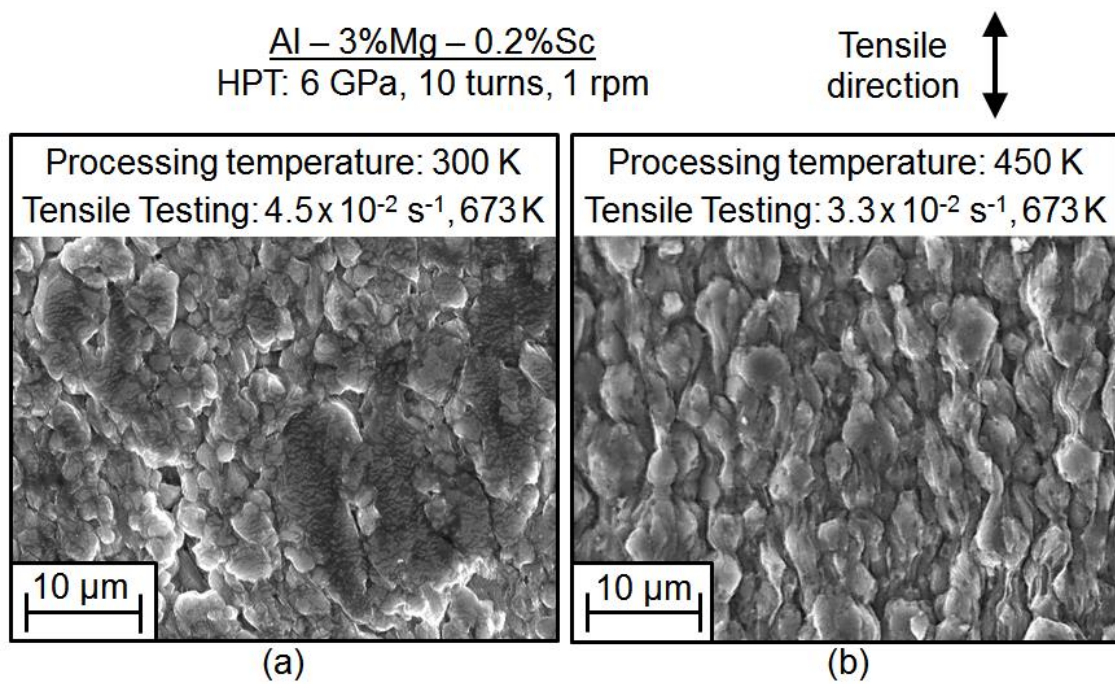


Fig. 3A. SE images taken along the gauge area of the fractured specimens of the Al-3Mg-0.2Sc alloy subjected to 10 HPT turns at (a) 300 and (b) 450 K and tested in tension at 673 K using similar strain rates.

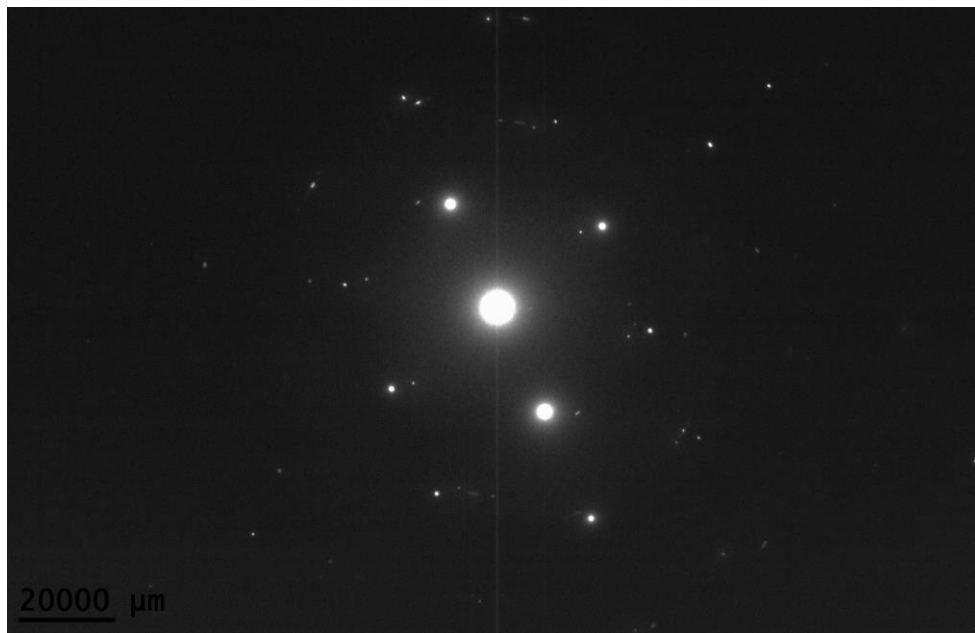


Fig. 4A. Diffraction pattern corresponding to an area having a large fraction of coherent Al_3Sc precipitates in the Al-3Mg-0.2Sc alloy processed by HPT at 450 K and further heated at 673 K.

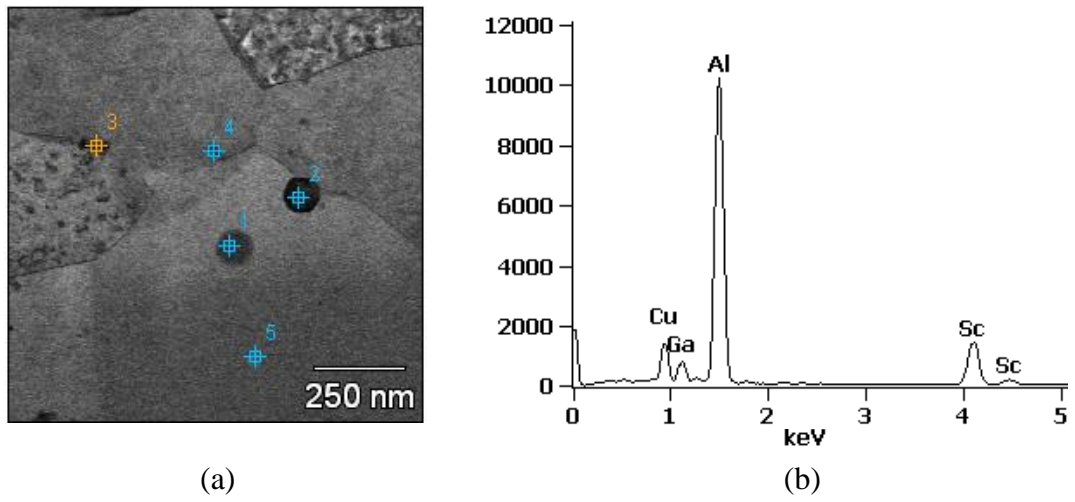


Fig. 5A. (a) STEM image and (b) corresponding EDS spectrum at P1 for an Al-3Mg-0.2Sc alloy processed by HPT at 450 K and further deformed at 673 K.